Simulated impacts of vertical distributions of black carbon aerosol on meteorology and PM$_{2.5}$ concentrations in Beijing during severe haze events

Donglin Chen[1], Hong Liao[1*], Yang Yang[1], Lei Chen[1], Delong Zhao[2], Deping Ding[2]

[1]Jiangsu Key Laboratory of Atmospheric Environment Monitoring and Pollution Control, Jiangsu Engineering Technology Research Center of Environmental Cleaning Materials, Collaborative Innovation Center of Atmospheric Environment and Equipment Technology, School of Environmental Science and Engineering, Nanjing University of Information Science & Technology, Nanjing, Jiangsu, China

[2]Beijing Weather Modification Office, Beijing 100089, China

*Correspondence to: Hong Liao (hongliao@nuist.edu.cn)

Abstract.

Vertical profiles of black carbon (BC) play a critical role in modifying the meteorological conditions such as temperature, planetary boundary layer height (PBLH), and regional circulation, which influence surface-layer concentrations of $PM_{2.5}$ (particulate matter with a diameter of 2.5 μm or less; surface-layer covers from 0 to 79.5 m). However, BC vertical profiles in current models usually have large uncertainties. In this study, by using measurements of BC vertical profiles in Beijing collected by King-Air350 aircraft and the Weather Research and Forecasting with Chemistry model (WRF-Chem) coupled with an improved integrated process (IPR) analysis scheme, we investigated the direct radiative effect (DRE) of BC with different vertical profiles on meteorology and $PM_{2.5}$ concentrations in Beijing during two severe haze events (11-12 December 2016 and 16-19 December 2016). Compared with measurements in Beijing, the model overestimated BC concentrations by 87.4% at the surface and underestimated BC mass by 14.9% at altitudes of 300-900 m as averaged over the two pollution events. The BC DRE with the default vertical profiles from the model heated the air around 300 m altitude but the warming would be stronger when BC vertical profiles were modified for each day using the observed data during the two severe haze events. Accordingly, compared to the simulation with the default vertical profiles of BC, PBLH was reduced further by 24.7 m (6.7%) and 6.4 m (3.8%) in Beijing in the first and second haze events, respectively, with the modified vertical profiles, and hence the surface-layer $PM_{2.5}$ concentrations were higher by 9.3 μg m^{-3} (4.1%) and 5.5 μg m^{-3} (3.0%) over central Beijing, owing to increased positive

40   contributions of vertical mixing and chemical processes. Furthermore, we quantified by

41   sensitivity experiments the roles of BC vertical profiles with six exponential decline

42   functions ($C(h)=C_0 \times e^{-h/hs}$ and hs=0.35, 0.48, 0.53, 0.79, 0.82 and 0.96) parameterized

43   on the basis of the observations. A larger hs means less BC at the surface and more BC

44   in the upper atmosphere, resulting in less solar radiation reaching the ground and

45   consequently a stronger cooling at the surface (+0.21 with hs of 0.35 vs. -0.13°C with

46   hs of 0.96). Our results indicate that it is very important to have accurate vertical

47   profiles of BC in simulations of meteorology and $PM_{2.5}$ concentrations during haze

48   events.

1. Introduction

With the rapid economic development and large increases in fossil energy consumption, haze pollution has become one of the most serious challenges in China, especially in the Beijing-Tianjin-Hebei (BTH) region (Wang et al., 2015; Zhang et al., 2019). In 2014 and 2015, the numbers of extremely serious $PM_{2.5}$ (particulate matter with an aerodynamic equivalent diameter of 2.5 μm or less) pollution days (with daily mean $PM_{2.5} > 150$ μg m^{-3}) in Beijing reached 45 and 54, respectively (He et al., 2017). The real-time hourly average concentration of $PM_{2.5}$ in Beijing even reached 1000 μg m^{-3} during the severe haze events in January 2013, far exceeding the Chinese Ambient Air Quality Grade I Standards (35 μg m^{-3} for daily mean $PM_{2.5}$) (Liu et al., 2017). With the implementation of the toughest-ever clean air policy since 2013, the observed annual mean $PM_{2.5}$ concentrations averaged over 74 cities in China fell from 61.8 μg m^{-3} in 2013 to 42.0 μg m^{-3} in 2017 (Zhang et al., 2016; Wang et al., 2017a; Li et al., 2019; Zhang et al., 2019). However, severe haze events still occurred in Beijing during the COVID-19 lockdown period (January-February 2020) (Huang et al., 2020; Zhu et al., 2020). Therefore, understanding the mechanisms responsible for the occurrence of severe haze is important for air quality management planning.

BC, an important component of $PM_{2.5}$, is emitted mainly from the incomplete combustion of fossil fuel, biofuel, and biomass burning. BC particles can strongly absorb solar radiation in the atmosphere, which alters the Earth's radiation balance (Bond et al., 2013; Huang et al., 2015; Hu et al., 2020). In recent years, researchers have found that the radiative effect of BC significantly affects the structure of planetary

72   boundary layer (PBL) during severe haze pollution events (Ding et al., 2016; Huang et

73   al., 2018; Wang et al., 2018; Liu et al., 2019). Ding et al. (2016) illustrated by using the

74   Weather Research and Forecasting model coupled with Chemistry (WRF-Chem) that

75   BC suppressed the development of PBL by heating the air in the upper PBL and

76   reducing the solar radiation at the surface in Beijing in December 2013. This process

77   was defined as the "dome effect" of BC by Ding et al. (2016). This "dome effect" was

78   also found over the Indian Ocean (Wilcox et al., 2016). BC can also change the land-

79   sea thermal contrast and induce circulation anomalies during severe haze events (Gao

80   et al., 2016b; Qiu et al., 2017; Ding et al., 2019a; Chen et al., 2021). Ding et al. (2019a)

81   showed by using the WRF-Chem model that, during a haze event in December 2013,

82   the direct radiative effect (DRE) of BC enhanced advection between land and sea by

83   causing a cooling (-1.0°C) in air temperature over land and a warming (+0.8°C) in air

84   temperature over sea, which transported moist air from the sea to the Yangtze River

85   Delta region. Qiu et al. (2017) and Chen et al. (2021) also reported by using the WRF-

86   Chem model that the radiative effect of BC induced strong anomalous northeasterly

87   winds from the sea during a haze event in North China Plain (NCP) in February 2014.

88   BC can influence concentrations of $PM_{2.5}$ during haze events because of its impact

89   on PBL and other meteorological fields (Gao et al., 2016b; Wilcox et al., 2016; Miao et

90   al., 2017; Qiu et al., 2017; Gao et al., 2018; Wang et al., 2019; Chen et al., 2021). Gao

91   et al. (2016b) used the WRF-Chem model to simulate the haze event that occurred in

92   the NCP in January 2010 and found a maximum increase in $PM_{2.5}$ of 14.4 $\mu g\ m^{-3}$ (5.1%)

93   due to the DRE of BC. Qiu et al. (2017) also analyzed the impact of BC on surface-

94   layer $PM_{2.5}$ during a haze pollution in NCP in February of 2014 by using the WRF-

95   Chem model and found that the average $PM_{2.5}$ concentration increased by 2.1 μg m^{-3}

96   (1.0%) owing to the DRE of BC. Chen et al. (2021) analyzed, by using the WRF-Chem

97   model, the DRE from the aging of BC and its impact on $PM_{2.5}$ concentration over the

98   BTH region during a haze event in February 2014. They found that the near-surface

99    $PM_{2.5}$ concentration average over BTH increased by 9.6 μg m^{-3} (7.0%) due to the aging

100   of BC.

101   So far few studies examined the impacts of vertical distributions of BC aerosol on

102   meteorology and $PM_{2.5}$ concentrations. Wang et al. (2018) examined the role of BC at

103   different altitudes in influencing PBL height (PBLH) by considering a single column

104   using the WRF-Chem version 3.6.1. They divided the height from 150 to 2250 m evenly

105   into 7 layers and increased BC concentrations from 0 to 30 μg m^{-3} with an increment of

106   2 μg m^{-3} at one of the layers with the BC concentrations at the other layers fixed to 0

107   μg m^{-3}. Model results showed that the near-surface BC could increase PBLH by 0% -

108   4%, while BC aloft would decrease PBLH by 2% - 16% due to the warming of

109   atmosphere by BC. Current chemistry-climate models were reported not to be able to

110   represent the BC vertical profiles accurately, so sensitivity studies were carried out to

111   adjust vertical profiles of BC in the model by changing the vertical resolution, aerosol

112   microphysical scheme and emission height (Wang et al., 2019; Yang et al., 2019;

113   Watson-Parris et al., 2019).

114   In recent years, measurements of BC vertical distribution have been conducted by

115   aircraft during the severe haze events in Beijing, using a single particle soot photometer

116   (SP2) (Zhao et al., 2018; Tian et al., 2019; Zhao et al., 2019; Tian et al., 2020; Liu et

117   al., 2020). During the period of severe pollution from 11 to 19 December 2016, Zhao

118   et al. (2019) collected BC vertical profiles over Beijing by Air350 aircraft and found

119   that the vertical profiles can be classified into two types. The first type was

120   characterized by decreases in BC concentration with altitude, which was the case

121   mainly controlled by local emissions. The second type had maximum BC concentration

122   around 900 hPa, which was mainly affected by regional transport from the polluted

123   south/southwest region. Generally, the first type occurred more frequently than the

124   second type during haze events in Beijing. Observations of vertical profiles of BC in

125   severe haze events over Beijing in 2018 by a King-Air350 aircraft by Ding et al. (2019b)

126   also obtained the same types of profiles.

127   In this work, we use the BC vertical profiles observed during two severe haze

128   events (11-12 December 2016 and 16-19 December 2016) over Beijing and the online-

129   coupled WRF-Chem model to investigate the DRE of BC vertical profiles on

130   meteorology and $PM_{2.5}$ concentrations. Compared with previous studies that examined

131   the impact of BC on meteorology and $PM_{2.5}$, our study is the first to pay attention to the

132   role of BC vertical profile as well as the underlying mechanism. The description of the

133   model, observational datasets and numerical experiments are presented in Section 2.

134   Section 3 evaluates simulated meteorological and chemical variables by comparing

135   with observations. Section 4 compares of the DRE of BC with original and modified

136   vertical profiles, and Section 5 discusses the role of BC vertical profiles in influencing

137   meteorological parameters and $PM_{2.5}$ concentrations. The conclusions of this study are

138   given in Section 6.

139

2. Method

2.1 Model configuration

142   A fully coupled online Weather Research and Forecasting with Chemistry model

143   (WRF-Chem version 3.7.1) (Grell et al., 2005; Skamarock et al., 2008) was employed

144   to simulate the two severe haze events in Beijing from 7 to 20 December 2016 and the

145   initial 4 days are spin-up. This model adopts Lambert projection and two nested

146   domains with grid resolutions of 30 km (domain 01) and 10 km (domain 02). Figure 1

147   shows that the outer domain covers the most of China with 100 (west-east) × 100

148   (south-north) grid cells and the second domain covers the BTH region with 58 (west-

149   east) × 76 (south-north) grid cells. The number of vertical layers is 29 with the first 15

150   layers below 2 km for finer resolution in the PBL. Meteorological initial and boundary

151   conditions in this model were derived from National Center for Environmental

152   Prediction (NCEP) Final (FNL) Operational Model Global Tropospheric Analyses

153   (ds083.2) with a spatial resolution of 1°×1°. MOZART-4 (Model for Ozone And

154   Related chemical Tracers-4) simulation results provided the initial and lateral boundary

155   conditions for the concentrations of chemical species in our model (Emmons et al.,

156   2010).

157   Anthropogenic emission data in year 2016 were obtained from the MEIC inventory

158   with a spatial resolution of 0.25º × 0.25º (Zheng et al., 2018). This inventory includes

159   sulfur dioxide (SO_2), nitrogen oxides (NO_x), carbon monoxide (CO), non-methane

volatile organic compounds (NMVOC), ammonia (NH_3), BC, organic carbon (OC),

$PM_{2.5}$, PM_{10} and carbon dioxide (CO_2), which were categorized into agriculture,

industry, residence, transport and power generation sectors (Li et al., 2015). The

biogenic emissions were calculated online using the MEGAN (Model of Emissions of

Gases and Aerosol from Nature), including isoprene, terpene and other substances

emitted by plants (Guenther et al., 2006). Biomass burning emissions were taken from

the Fire INventory from NCAR (FINNv1.5) which provides daily emissions at a

horizontal resolution of ~1 km^2 (Wiedinmyer et al., 2011).

The parameterization schemes of physical and chemical processes of WRF/Chem

model adopted in the study are summarized in Table 1. The Carbon-Bond Mechanism

version Z (CBMZ) is chosen to simulate the gas-phase chemistry. The aerosols scheme

is the Model for Simulating Aerosol Interactions and Chemistry (MOSAIC) which

includes sulfate, nitrate, ammonium, chloride, sodium, BC, OC and other inorganic

aerosol, and the aerosol particles are divided into 8 particle size segments. However,

the formation of secondary organic aerosol is not considered in this scheme (Zhang et

al., 2012; Gao et al., 2016a). In MOSAIC, the aerosol particles are assumed to be

internal mixture and aerosol optical properties are calculated by the volume averaging

mixing method (Barnard et al., 2010; Stelson, 1990). The choice for photolysis schemes

is Fast-J photolysis scheme.

2.2 Integrated process rate (IPR) analysis

The IPR analysis has been widely applied to illustrate the impacts of each

physical/chemical process on the variations in O_3 concentrations (Zhang and Rao, 1999;

182 Jiang et al., 2012; Gao et al., 2017; Gao et al., 2018). The improved IPR analysis method

183 developed by Chen et al. (2019) in WRF-Chem model is used in this work to

184 quantitatively analyze the contributions of physical/chemical processes to $PM_{2.5}$

185 concentrations, including the contributions from the sub-grid convection (CONV),

186 vertical mixing (VMIX), chemistry (CHEM), regional transport (TRA), wet scavenging

187 (WET), emission source (EMI) and other processes (OTHER). CONV refers to the

188 transport within the sub-grid wet convective updrafts, downdrafts, and precipitation

189 (Chen et al., 2019) and VMIX is affected by atmospheric turbulence and vertical

190 distribution of $PM_{2.5}$ concentrations (Zhang and Rao, 1999; Gao et al., 2018). CHEM

191 represents $PM_{2.5}$ production and loss including gas-phase, cloud and aerosol chemistry.

192 TRA is caused by advection, which is highly related to wind and horizontal distribution

193 of $PM_{2.5}$ concentrations (Gao et al., 2018; Chen et al., 2019). WET represents the wet

194 removal processes of aerosols by in-cloud scavenging and below-cloud washout. EMI

195 is controlled by emission source. OTHER represents the processes other than the above

196 6 processes in the model. The NET is the sum of all physical and chemical processes,

197 which matches the variations in $PM_{2.5}$ concentrations. It is worth noting that each IPR

198 variable is an accumulated value which is the sum of each time step.

2.3 Observational data

200   To evaluate the model performance in simulating near-surface meteorological

201 fields, the observed hourly temperature at 2 m (T2), relative humidity at 2 m (RH2),

202 wind speed at 10 m (WS10) and wind direction at 10 m (WD10) at Beijing-Capital

203 International Airport station (40.08°N, 116.58°E) are collected from NOAA's National

Climatic Data Center (http://gis.ncdc.noaa.gov/maps/ncei/cdo/hourly). Due to the limited observations of planetary boundary layer heights (PBLH), shortwave downward radiation flux (SWDOWN) and total cloud cover in Beijing, the reanalysis data of 3-hourly PBLH, SWDOWN and total cloud cover for Beijing from the Global Data Assimilation System (GDAS) with a spatial resolution of $1° \times 1°$ (http://ready.arl.noaa.gov/READYamet.php) were used for model evaluation. More details about the GDAS dataset can be found in Rolph (2013) and Kong et al. (2015). The radiosonde data (temperature and relative humidity profiles) in Beijing were obtained from the University of Wyoming, Department of Atmospheric Science (http://weather.uwyo.edu/upperair/sounding.html). Hourly concentrations of $PM_{2.5}$, CO, NO_2, SO_2 and O_3 at Beijing Station were obtained from the China National Environmental Monitoring Center (CNEMC, http://www.cnemc.cn/), which were used to evaluate the model performance in simulating pollutants at the surface. Aerosol optical depth (AOD) at 550 nm over China retrieved from MODIS (Moderate Resolution Imaging Spectroradiometer) satellite was used to evaluate the horizontal distribution of simulated optical properties of aerosols in this study (https://ladsweb.modaps.eosdis.nasa.gov/). The MYD03 (Level-1A) product with 1 km spatial resolution from Aqua platform and the MOD03 (Level-1A) product with 1 km spatial resolution from Terra platform were used in this study. The values of daily aerosol optical depth (AOD) at 500 nm and 675 nm in Beijing were obtained from the AERONET data set (https://aeronet.gsfc.nasa.gov/).

The vertical profiles of BC mass concentrations in Beijing were collected by King-

226 Air350 aircraft using SP2 during 11-12 and 16-19 December 2016. The aircraft

227 departured from Shahe (~20 km to the central Beijing) (Fig. 1) at 12:00-13:00 local

228 time (LT) and returned during 15:00-16:00 LT, which avoided the possible diurnal

229 variation of the PBL among flights. Most flights could reach 2.5 km. Zhao et al. (2019)

230 reported that these vertical profiles of BC could be expressed as an exponential decline

231 function $C(h) = C_0 e^{-\frac{h}{hs}}$ except 11 December 2016, where $C(h)$ (μg m^{-3}) is BC

232 concentration at altitude h (km), C_0 (μg m^{-3}) is BC concentration at the surface, and

233 each hs value is calculated for each flight of BC vertical profile using nonlinear

234 regression (Table S1). Tian et al. (2019) observed a regional transport of pollution in

235 Beijing from 10 to 12 December 2016 using SP2 and they found a different vertical

236 structure of BC from that of Zhao et al. (2019), with the BC concentration at the

237 altitudes of 400-900 m being 1.5 times higher than the near-surface BC concentration

238 on 11 December 2016. More detailed information about King-Air350 aircraft dataset

239 can be found in Zhao et al. (2019), Ding et al. (2019b) and Tian et al. (2019).

240 **2.4 Numerical experiments**

241   To compare the DRE of BC with original and corrected vertical profiles and

242 quantify the role of BC vertical profiles in influencing meteorological conditions and

243 air pollutants, we performed the following numerical experiments as summarized in

244 Table 2.

245 1. CTRL: The control simulation with the direct and indirect radiative effects of all

246 aerosols (BC, OC, sulfate, nitrate, ammonium, Na$^+$, Cl$^-$ and OIN) included for the time

247 period of 11-20 December 2016. The vertical profiles of BC were the default ones

248 simulated by the model.

249 2. NoBCrad: The same as the CTRL simulation, except that the DRE of BC was turned

250 off.

251 3. VerBC_obs: The same as the CTRL simulation, except that the BC vertical profiles

252 in the model were modified according to the observed ones. The specific method will

253 be discussed below.

254 4. VerBC_hs1-6: The same as the CTRL simulation, except that the vertical profiles of

255 BC in the model were modified according to the exponential decline function

256 ($C(h)=C_0 \times e^{-h/hs}$). The values of hs in VerBC_hs1 to VerBC_hs6 were 0.35 to 0.96 (from

257 small to large), respectively.

258 5. VerBC_RT: The same as the VerBC_hs1-6 simulations, except that the BC vertical

259 profiles in the model were modified according to the observed transport BC vertical

260 profile on 11 December 2016 which was affected by regional transport.

261   In the case of NoBCrad, the BC DRE was turned off by setting the BC mass

262 concentration equal to zero when calculating the optical properties of BC, following the

263 studies of Qiu et al. (2017) and Chen et al. (2021). In VerBC_obs experiment, we

264 modified the simulated BC vertical profile online using the observed BC vertical profile

265 on the corresponding day. Firstly, we interpolated the observed BC concentrations to

266 the height of each layer in the model as $C_{obs\_int(i)}$. Each layer in the model has a top

267 height and a bottom height and we selected the middle height of this layer for

268 interpolation. Secondly, we used $C_{obs\_int(i)}$ to calculate the BC mass column burden in

269 each layer ($M_{obs\_int(i)}$) in the model, and $P_{obs\_int(i)}$ is the percentage of BC mass column

270   burden in each layer to the total BC mass column burden (Fig. S1) calculated by

271    $M_{obs\_int(i)} = C_{obs\_int(i)} * (H_{sim\_top(i)} - H_{sim\_bot(i)})$ (1)

272   where $H_{sim\_top(i)}$ is the top height of layer i and $H_{sim\_bot(i)}$ is the bottom height of layer i.

273    $P_{obs\_int(i)} = \frac{M_{obs\_int(i)}}{\sum_{i=1}^{16} M_{obs\_int(i)}} * 100\%$ (2)

274

275   In the VerBC_obs simulation, the simulated BC mass column burden was redistributed

276   to each layer below 2.5 km according to the calculated $P_{obs\_int(i)}$. These procedures

277   ensure that the modification of BC vertical profile for each day in the model by using

278   the observed data does not change the total BC mass column burden. Since the aircraft

279   measured only BC concentrations below 2.5 km, we modify BC profile up to the 16th

280   model layer (about 2.5 km in Beijing).

281   In the experiment of VerBC_hs1~6, we also used the above method to modify the

282   BC vertical profile by an exponential decline function which is $C(h)=C_0 \times e^{-h/hs}$.

283   However, in cases of VerBC_hs1~6, we modified for the dates of 12 and 16-19

284   December. On December 11, BC did not show an exponential decline with height due

285   to the regional transport. In simulation of VerBC_RT, the method and setting were the

286   same as VerBC_hs1~6, except that the BC vertical profile in the model was modified

287   according to the observed one on 11 December 2016. In VerBC_obs, VerBC_hs1~6 and

288   VerBC_RT cases, the modifications of BC vertical profiles were performed only when

289   the direct radiative forcing of BC was calculated. All other physical and chemical

290   processes in these experiments still used the original BC vertical profiles simulated by

291   the model. The BC vertical profiles were only modified in the blue square shown in Fig.

292   1a.

3 Model evaluation

3.1 Near-surface air pollutants and BC vertical profiles

Figures 2a-2i show the horizontal distributions of simulated surface-layer $PM_{2.5}$ concentrations at 2 pm LT from 11 to 19 December 2016. In Beijing, high $PM_{2.5}$ concentrations of 234.1 and 165.9 $\mu g\ m^{-3}$ occurred on December 11 and 12, respectively. The severe pollution in Beijing on December 11 was caused by regional transport from the southern heavily polluted area under a prevailing southerly air flow (Tian et al., 2019). From December 16, $PM_{2.5}$ started to accumulate in the eastern China and the concentrations of $PM_{2.5}$ reached highest value of 217.8 $\mu g\ m^{-3}$ on 19 December in Beijing. The daily $PM_{2.5}$ concentrations (Fig. 2j) in Beijing had low values during 13-15 December 2016. The model results for Beijing in this paper are the averages over the region of blue square shown in Fig. 1a unless stated otherwise. The severe pollution during 16-19 December 2016 was mainly affected by local emissions. We are mainly focused on the two heavy pollution incidents (11-12 and 16-19 December 2016) in the following sections.

Results from the CTRL simulation were compared with the observed hourly surface concentrations of $PM_{2.5}$, NO_2, O_3, CO and SO_2 during 11-19 December 2016 in Beijing in Fig. 3. The observed maximum $PM_{2.5}$ concentration of 219.5 $\mu g\ m^{-3}$ occurred on December 18, far exceeding the national air quality standard for daily $PM_{2.5}$ of 75 $\mu g\ m^{-3}$ (Wang et al., 2017a). The correlation coefficient (R), mean bias (MB), normalized mean bias (NMB) and mean fraction bias (MFB) are summarized in Table

314 3. The model can reasonably reproduce the temporal variations of $PM_{2.5}$, NO_2, O_3 and

315 CO; the correlation coefficients between simulated and observed hourly concentrations

316 are 0.77, 0.78, 0.66 and 0.73, respectively. The correlation coefficient for SO_2 is lower

317 (0.38). Gao et al. (2016b) explained that WRF-Chem model cannot represent well the

318 SO_2 concentration and its change with time due to the uncertainty in SO_2 emissions and

319 missing heterogeneous oxidation. Compared with observations, the model

320 overestimates the concentrations of $PM_{2.5}$ and NO_2 in Beijing with the MBs and NMBs

321 of (13.2 μg m^{-3}, 10.0%) and (8.5 ppbv, 21.6%), respectively, and underestimates the

322 concentrations of O_3 (-0.1 ppbv, -1.2%) and CO (-0.1 ppmv, -4.9%). It should be noted

323 that the model performance in simulating $PM_{2.5}$, SO_2, CO and O_3 is better during the

324 two haze events than on clean days. For hourly $PM_{2.5}$, for example, the MBs (NMBs)

325 are 29.1 μg m^{-3} (82.5%) on clean days and 6.3 μg m^{-3} (3.5%) during the two haze events.

326 The possible reasons for the overall overestimation of $PM_{2.5}$ are as follows: (1) the

327 model biases in underestimating WS10 and daytime PBLH; (2) the uncertainties in

328 anthropogenic emission data (e.g. the overestimation in the BC emissions) (Qiu et al.,

329 2017; Chen et al., 2021). Overall, the model can capture fairly good the two severe

330 pollution events in Beijing during 11-19 December 2016.

331 Because of the lack of measured BC vertical profiles from 13-15 December 2016

332 in Beijing, Figure 4 compares only the simulated vertical profiles of BC with

333 observations for the two polluted events (11-12 and 16-19 December 2016). Observed

334 mass concentrations of BC decreased exponentially with altitude in all days except for

335 December 11 when regional transport of pollution dominated. On December 11, the

336 observed maximum mass concentration of BC (7.0 μg m^{-3}) occurred at 850 m altitude,

337 which was much higher than the surface-layer concentration of 4.7 μg m^{-3}. Compared

338 with the observed vertical profiles of BC, the model can well represent the decreases of

339 BC mass concentration with height on December 12 and 16-19, but cannot reproduce

340 the vertical profile on December 11. Possible reasons for model's failing to represent

341 BC vertical profile on December 11 are as follows: (1) the model cannot capture the

342 wind at high altitudes and does not reproduce the high-altitude BC concentrations in

343 the surrounding areas of Beijing; (2) the model underestimates the daily maximum

344 PBLH in Beijing which inhibits the upward transport of surface-layer BC. Averaged

345 over the two pollution events, the simulated BC mass concentration was overestimated

346 by 87.4% on the ground and underestimated by 33.1% at altitude of 1000 m compared

347 with the observations in Beijing. The inaccuracy of the vertical distribution of BC

348 would lead to inaccurate representation of the interactions between BC and PBL,

349 especially in heavily polluted events.

350 ## 3.2 Meteorological parameters

351 The first haze event started on December 11 when southeasterlies transported

352 polluted air from southern BTH to Beijing (Fig. 2a). Although the southeasterlies turned

353 into northeasterlies in Beijing on December 12, PM$_{2.5}$ concentrations were still high

354 because of the high relative humidity (63.2%) that was conductive to the formation of

355 secondary aerosols. With the relatively high wind speed of 3.6 m s^{-1} and low relative

356 humidity of 37.2% in Beijing during 13-15 December, the haze pollution gradually

357 disappeared (Fig. 2c-2e). From 16 to 19 December, PM$_{2.5}$ began to accumulate again

358 with unfavorable diffusion conditions (WS10 of 1.4 m s^{-1}) and enhanced formation of

359 secondary aerosols under high relative humidity of 67.1% (Li et al., 2019; Dai et al.,

360 2021). Throughout the simulated period of 11-19 December 2016, Beijing had no

361 precipitation and was partly cloudy (Fig. 5g-5h). Figure 5 shows the hourly simulated

362 and observed T2, RH2, WS10, WD10,PBLH, SWDOWN, precipitation and total cloud

363 cover in Beijing from 11 to 19 December 2016. The statistical metrics are summarized

364 in Table 3. In the two severe haze events, the observed maximum RH2 in each day

365 exceeded 70.0%, which accelerated the formation of secondary aerosols (Sun et al.,

366 2006; Wang et al., 2014). Compared with the observations, the model can well represent

367 the temporal variation of T2 and RH2 with correlation coefficients of 0.77 and 0.75,

368 respectively, but slightly overestimates T2 with a MB of 0.1 ℃ and underestimates RH2

369 with a MB of 3.4%. For WS10, observations and simulated results both show low wind

370 speed with the mean values of 1.5 and 1.4 m s^{-1} in Beijing during the two periods of

371 haze events. Such meteorological condition was very beneficial to the accumulation of

372 near-surface pollution. The WRF-Chem model also captures the high values of WS10

373 from 14 to 15 December. For wind direction at 10 m, the NMB is -9.0% and the R is

374 0.45, which indicates that the model can simulate the change of wind direction during

375 the period of heavy pollution. For PBL, the reanalysis PBL was 118.7 m during the two

376 severe haze events, compared to 287.5 m during the clean period. The model can

377 represent the change of PBLH in Beijing from 11 to 19 December 2016 with R of 0.72.

378 The model overestimates PBLH by 30.9 m (17.7%) in Beijing as averaged over 11-19

379 December 2016. The overestimation is mainly in hours of 0:00-8:00 LT and 17:00-

380 23:00 LT. It is noted that the reanalysis PBLH values provided by GDAS of NOAA

381 were mostly 50-60 m at 0:00-8:00 LT and 17:00-23:00 LT in Beijing, far below the

382 simulated mean value of 154.5 m in these hours. There might be biases in the PBLH

383 from GDAS. Several previous studies showed that the values of observed PBLH from

384 Lidar measurements were about 200 m at night during haze events (Wang et al., 2012;

385 Luan et al., 2018; Chu et al., 2019). The simulated SWDOWN in CTRL experiment

386 agrees well with the observations with R and MB of 0.76 and -14.9 W m^{-2}. Due to the

387 limitation of the model outputs, the model provides only information of whether there

388 is cloud in the grid or not. The model can reproduce well the presence of cloud during

389 11-19 December 2016. Both observations and model results show no precipitation in

390 the studied time period.

391   The simulated and observed vertical profiles of temperature in Beijing during 11-

392 19 December 2016 are shown in Fig. S2. The observed temperature vertical profiles are

393 available only at 8:00 and 20:00. During the two severe pollution events, strong

394 temperature inversions below 1500 m were observed in Beijing, which inhibited

395 vertical mixing and caused the accumulation of pollutants near the ground. The model

396 captures these temperature inversions well but overestimates the inversion layer height

397 on December 11 and underestimates the inversion layer height from 16 to 19 December.

398 The inaccuracy of the simulated inversion layer height may be due to the fact that the

399 model cannot correctly represent the vertical profiles of BC (Fig. 4).

400 **3.3 AOD and AAOD**

401   AOD (AAOD) is the measure of aerosols (absorbing aerosols) distributed within a

402 column of air from the surface to the top of the atmosphere (Khor et al., 2014). Figure

403 S3 shows the horizontal spatial distributions of observed and simulated AOD at 550 nm

404 over the NCP averaged over 11-19 December 2016. The model can generally reproduce

405 the horizontal distribution of AOD, with a spatial correlation coefficient of 0.89.

406 However, the model underestimates AOD over the NCP region. Many previous studies

407 have shown that MODIS retrieval tends to overestimate AOD over NCP (Li et al., 2016;

408 Qiu et al., 2017). We also compared the simulated hourly AAOD at 550 nm with

409 AERONET AAOD in Beijing and Xianghe station in Fig. 6. The correlation coefficient

410 between simulations and observations is 0.85. Compared with AERONET AAOD,

411 simulated AAOD values at Beijing and Xianghe are overestimated by 0.02 (33.3%) and

412 0.02 (39.9%), respectively.

4. A comparison of BC DRE with original and modified vertical profiles

415 As shown in Fig. 4, the model does not represent well the vertical distribution of

416 BC concentrations during the two heavily polluted events, especially on December 11.

417 So, in this section, we examine the differences in the BC DRE on meteorology and

418 concentrations of pollutants with the original and modified vertical profiles.

4.1 Direct radiative effect of BC on meteorology

420 Figure 7 shows the atmospheric temperature and PBLH simulated from the CTRL

421 simulation and their changes caused by BC DRE with original profiles (CTRL minus

422 NoBCrad) and modified profiles (VerBC_obs minus NoBCrad), over Beijing from 11

423 to 19 December 2016. Light-absorbing BC heated the air at around 300 m on December

424 11 and 16-19, regardless of the original or modified BC vertical profiles (Fig. 7b and

425 7c). With the original and modified BC profiles, the maximum warming effects in the

426 PBL were 0.8℃ and 0.9℃, respectively, at 14:00 LT on December 18. Although BC

427 concentration was the highest at the surface, the largest increase in temperature

428 occurred in the upper layers because of the stronger shortwave absorption efficiency of

429 BC at higher altitude (Ding et al., 2016; Wang et al., 2018). The warming at around 300

430 m resulted in a more stable stratification, thereby weakening convective motions (Gao

431 et al., 2018). The largest reductions in PBLH were 133.8 m (28.0%) at 14:00 LT on

432 December 12 and 141.2 m (59.0%) at 14:00 LT on December 18 in Beijing with original

433 and modified BC vertical profiles, respectively. On December 11 when regional

434 transport of pollution dominated, relative to the simulation with original BC profile,

435 simulated air temperature with modified profile was lower by about 0.5℃ within the

436 PBL (Fig. 7d), which was caused by the observed maximum mass concentration of BC

437 around 850 m altitude (Fig. 4a). Correspondingly, the maximum reduction in PBLH of

438 74.2 m was also simulated on December 11. On December 16-19 when local emissions

439 dominated, compared the effects of original BC profiles, the air temperatures at around

440 300 m were all higher with modified BC. The largest difference of +0.1℃ was

441 simulated in the PBL on December 18 (Fig. 7d).

442 Figure 8 shows the spatial distributions of changes in T2, sea-level pressure (SLP)

443 and wind at 10 m caused by BC DRE with original and modified vertical profiles. BC

444 DRE with both original and modified vertical profiles produced anomalous

445 northeasterlies in eastern BTH during the two haze events. The mechanism of such

446   changes is that BC DRE induced a strong warming over the Bohai Sea in the east of

447   BTH with a maximum warming of about 1.8°C, resulting in an anomalous low-pressure

448   here and consequently anomalous northeasterlies in eastern BTH (Fig. 8c-8d). The

449   similar changes in winds caused by the heating effect of BC were also reported in

450   previous studies (Gao et al., 2016b; Qiu et al., 2017; Chen et al., 2021).

451   4.2 Direct radiative effect of BC on PM$_{2.5}$ concentration

452   By altering the meteorological conditions, BC exerts feedback onto PM$_{2.5}$

453   concentrations. Figure 9 illustrates the impacts of BC DRE with original and modified

454   vertical profiles on surface-layer PM$_{2.5}$ as well as the differences in simulated surface-

455   layer PM$_{2.5}$ between VerBC_obs and CTRL (VerBC_obs minus CTRL) in Beijing

456   during the two haze events. Because of the differences in BC-induced changes in air

457   temperature, wind field, and PBLH, changes in surface-layer PM$_{2.5}$ concentrations in

458   the northern and southern Beijing were different. In the first haze event of 11-12

459   December, although PBLH was reduced in the northern Beijing due to BC DRE,

460   enhanced northerlies brought in relatively clean air to northern Beijing, leading to

461   decreases in surface-layer PM$_{2.5}$ concentrations with maximum values of 12.5 μg m^{-3}

462   (9.4%) and 10.6 μg m^{-3} (8.0%) in this region with the original and modified BC vertical

463   profiles, respectively. Nevertheless, PM$_{2.5}$ concentrations increased by up to 17.8 μg m^{-}

464   ^{3} (6.6%) and 24.0 μg m^{-3} (9.3%) in the southern Beijing due to BC effect with original

465   and modified vertical profiles, respectively. In the second haze event of 16-19

466   December, the surface-layer PM$_{2.5}$ concentrations increased in most areas of Beijing

467   with both vertical profiles. Compared to the simulation with the original profiles, the

468   modified profiles of BC led to larger increases in $PM_{2.5}$ concentrations over Beijing,

469   and the maximum differences in $PM_{2.5}$ were simulated over central Beijing, which were

470   9.3 μg m^{-3} (3.6%) and 5.5 μg m^{-3} (3.1%) in the first and second haze events, respectively.

471   To explain the changes in surface-layer $PM_{2.5}$ concentrations in Beijing due to BC

472   effects, we carried out process analysis for $PM_{2.5}$ for 12:00-18:00 of each day when the

473   DRE of BC is the largest (Figs. 9a3, 9b3, and 9c3). From 11 to 19 December 2016,

474   VMIX had dominant positive contribution to changes in $PM_{2.5}$ concentration, which

475   reached the maximum contributions of 32.4 μg m^{-3} and 33.9 μg m^{-3} on December 18

476   with original and modified BC vertical profiles, respectively. The vertical mixing was

477   strongly restrained by PBLH, therefore, the decreases in PBLH caused accumulation of

478    $PM_{2.5}$ in the lower layers. Meanwhile, CHEM contributed 4.8 μg m^{-3} and 6.1 μg m^{-3} to

479    $PM_{2.5}$ changes because more aerosol precursors restrained in the boundary layer led to

480   the formation of secondary particles. TRA was the major process that had negative

481   contribution to the changes in $PM_{2.5}$, which can be explained by the enhanced

482   northerlies in the central part of NCP due to BC effects as shown in Fig 8. Relative to

483   the case with original BC vertical profiles, VMIX and CHEM contributions increased

484   largely with modified profiles, with increases of 8.6 μg m^{-3} (6.5%) and 7.7 μg m^{-3}

485   (26.8%), respectively, as averaged over the two haze events, reflecting the further

486   decreases in PBLH (Fig. 7d).

487   Figure 10 shows the vertical profiles of the contributions of physical/chemical

488   processes to changes in $PM_{2.5}$ over Beijing due to BC DRE with original (CTRL minus

489   NoBCrad; Figs. 10a1 and 10b1) and modified vertical profiles (VerBC_obs minus

490   NoBCrad; Figs. 10a2 and 10b2) in the two haze events. In the first haze event of 11-12

491   December when regional transport of pollution dominated, the NET contribution to

492    $PM_{2.5}$ was positive below 256 m, because of the positive contribution of VMIX was

493   larger than the negative contribution of TRA. However, in the upper layers (from 256

494   to 1555 m), the contributions of VMIX and CHEM became negative with both original

495   and modified vertical profiles, which can be explained by the decreases in PBLH

496   inhibiting the transport of low-layer pollutants to the upper layer. Compared to the

497   original BC vertical profiles, the modified BC vertical profiles increased $PM_{2.5}$ in the

498   entire vertical layers below 2080 m, in which the positive contribution between 256-

499   757 m was caused by TRA. These results agree with the observed high concentrations

500   of BC at altitudes of 600-1500 m on December 11 (Fig. 4a). In the second haze event,

501   the NET contribution to $PM_{2.5}$ was positive below 127 m and negative at 127-504 m.

502   However, the effects of BC on $PM_{2.5}$ were small above 504 m because BC

503   concentrations decreased rapidly with altitude.

504 4.3 Model performance in simulating meteorology and $PM_{2.5}$ with the

505 original and modified BC vertical profiles

506   It is of interest to compare the performance of CTRL (with original BC vertical

507   profiles) with that of VerBC_obs (with modified BC vertical profiles) in simulating

508   meteorological parameters and $PM_{2.5}$ during the two haze events. Figure S4 shows the

509   comparisons between observed T2, RH2, WS10, WD10, PBLH and the simulated

510   values from the CTRL and VerBC_obs simulations in Beijing in the two haze events

511   (11-12 December and 16-19 December 2016). Relative to CTRL simulation with

original BC vertical profiles, VerBC_obs simulation with modified BC vertical profiles

has better performance in simulating T2, WS10 and PBLH except for WD10 and RH2

in the first pollution event. While the MBs of T2, RH2, WS10, WD10 and PBLH are

0.2°C, 0.0%, -0.4 m s^{-1}, 3.8°, and 45.0 m in CTRL, they are 0.0°C, 2.2%, -0.1 m s^{-1},

10.9°, 29.0 m in VerBC_obs, respectively (Table S3). In the second pollution event, the

positive bias in PBLH (MB=43.7 m, NMB=42.9%) in CTRL is reduced to 33.9 m and

33.3% in VerBC_obs.

Table S4 shows the statistical comparison between observed hourly surface-layer

PM$_{2.5}$ and the model results from CTRL and VerBC_obs in Beijing for each day during

the two haze events. The model with modified BC vertical profiles can enhance the

capability in simulating the temporal variation of PM$_{2.5}$ for each day; the correlation

coefficient between simulated hourly concentrations and hourly observations in each

day of the studied period increased from 0.04-0.84 in CTRL to 0.24-0.93 in VerBC_obs.

5. Roles of BC vertical profiles

BC has higher light-absorbing efficiency at higher altitudes (Ding et al., 2016;

Wang et al., 2018). As described in Section 2.3, the observed vertical profiles of BC on

heavily polluted days (12 and 16-19 December) can be parameterized as exponential

decline functions using nonlinear regression ($C(h)=C_0\times e^{-h/hs}$) with hs values of 0.35,

0.48, 0.53, 0.79, 0.82 and 0.96, and the profiles affected by regional transport had high

concentrations of BC at high altitudes. We conducted seven sensitivity experiments

which applied six exponential functions and one observed transport-dominated vertical

profile, as described in Section 2.4, to examine the roles of BC vertical profiles in

534   influencing meteorological conditions and PM$_{2.5}$ during severe haze events. In these

535   sensitivity experiments, we only modify the BC vertical profiles for the dates of 12 and

536   16-19 December. In the function of $C(h)=C_0 \times e^{-h/hs}$, a larger hs means less BC at the

537   surface and more BC in the upper atmosphere, as shown in Fig. 11.

5.1 Impacts of BC vertical profiles on meteorology

539   Figure 12 shows the simulated changes in atmospheric temperature induced by BC

540   DRE with exponential functions (VerBC_hs1-6 minus NoBCrad) and with the

541   transport-dominated vertical profile (VerBC_RT minus NoBCrad). BC had a significant

542   warming effect at altitudes of 256-421 m from 12:00 to 18:00 (Fig. 7). Generally, with

543   the value of hs gradually increasing, the BC-induced warming in the afternoon around

544   300 m became smaller, which can be explained by the highest mass fraction of BC at

545   the altitudes of 256-421 m to total BC column burden in VerBC_hs1 case (31.7%) and

546   the lowest percentage in VerBC_hs6 case (21.7%) among the six sensitivity

547   experiments (Fig. S1). The maximum warming around 300 m was 0.42°C in VerBC_hs1

548   case and 0.19°C in VerBC_hs6 case. It should be noted that BC led to a significant

549   cooling effect at the surface (below 80 m) when hs values were 0.79, 0.82 and 0.96,

550   with the changes in temperature by -0.08, -0.09 and -0.13°C, respectively. Because

551   more BC mass was assigned into high altitudes (above 1000 m) with higher hs, less

552   solar radiation could reach the ground (Fig. S5). These results are consistent with those

553   found in previous modeling and observational studies (Cappa et al., 2012; Ferrero et al.,

554   2014; Ding et al., 2016; Wang et al., 2018). Meanwhile, in the case of VerBC_RT, BC

555   also had a cooling effect of -0.30°C at the surface (Fig. 12g). In current regional air

quality models, the uncertainties in BC profiles could influence the capability of a

model to simulate a cooling effect of BC on surface-air temperature (Wang et al., 2019).

We further use the difference in temperature between the upper PBL (T_H; 256-421

m) and the ground (T_L; 0-127 m) ($\Delta T_{BC} = T_H - T_L$) averaged over 12:00-18:00 LT of 12

and 16-19 December to quantify temperature inversion caused by BC DRE. BC aerosol

leads to cooling at the surface and warming in the upper PBL, both of which weaken

the convection in the boundary layer and consequently reduce the PBLH (Ding et al.,

2016; Wang et al., 2018; Chen et al., 2021). In our study, with hs values increasing from

0.35 to 0.96, ΔT_{BC} increased from 0.17 to 0.42°C, and the ΔT_{BC} value was 0.51°C in

VerBC_RT case (Fig. 13a). The larger ΔT_{BC} indicates stronger cooling at the surface,

such temperature inversion at 12:00-18:00 LT resulted in more stable stratification and

further inhibited the development of PBL. The cooling at the surface also reduced

sensible heat flux from the surface (Fig. S5), suppressing vertical turbulence and hence

reducing PBLH (Wilcox et al., 2016). As a result, the reductions in PBLH were larger

with higher hs (Fig. 13b). The minimum decrease in PBLH was -31.9 m (-14.3%) with

hs value of 0.35 and the maximum decrease was 48.9 m (22.0%) with hs value of 0.96,

as averaged the period of 12:00-18:00 of 12, 16-19 December. In the case of VerBC_RT,

the mean PBLH was reduced by 56.9 m (25.6%) during the period of 12:00–18:00.

5.2 Impacts of BC vertical profiles on PM$_{2.5}$ concentration

Figure 14a shows the changes in surface-layer PM$_{2.5}$ concentration caused by BC

DRE with six exponential functions (VerBC_hs1-6 minus NoBCrad) and the transport-

dominated vertical profile (VerBC_RT minus NoBCrad) averaged over 12 December

578 and 16-19 December 2016. From 0:00 to 11:00, the surface-layer $PM_{2.5}$ exhibited larger

579 BC-induced decreases with a higher value of *hs*. This can be explained by the negative

580 contribution of TRA process that increased during the period of 0:00-5:00 (Figs. 14b

581 and 14c) when *hs* value changed from 0.35 to 0.96. The surface-layer $PM_{2.5}$

582 concentration was reduced by up to 9.1 μg m^{-3} (6.2%) and 12.6 μg m^{-3} (8.6%) at 5:00

583 with *hs* values of 0.35 and 0.96, respectively. Compared to the NoBCrad case, the

584 surface-layer $PM_{2.5}$ concentrations were reduced by up to 13.8 μg m^{-3} (9.4%) at 5:00

585 due to BC DRE in VerBC_RT case. From 12:00 to 18:00, the BC-induced increase in

586 surface-layer $PM_{2.5}$ concentrations was larger as *hs* values were higher; relative to

587 NoBCrad simulation, the mean $PM_{2.5}$ concentrations were increased by 5.5 μg m^{-3}

588 (3.4%) and 7.9 μg m^{-3} (4.9%) with the *hs* values of 0.35 and 0.96, respectively. Because

589 the PBL was suppressed by BC DRE from 12:00 to 15:00, the contributions of VMIX

590 and CHEM to surface-layer $PM_{2.5}$ were positive and larger in magnitude than the

591 negative contribution of TRA. The NET of all processes was negative from 16:00 to

592 18:00 due to the continuous growth of negative contribution of TRA. The negative

593 contribution of TRA process from 12:00 to 18:00 can be explained by the enhanced

594 northerlies in the central part of BTH caused by BC DRE, which transported cleaner

595 air mass into Beijing (Fig S6). From 19:00 to 23:00, the surface-layer $PM_{2.5}$

596 concentrations were decreased by BC DRE, which can be explained by the dominant

597 negative contribution of TRA from 19:00 to 21:00. At 22:00, the reduction in surface-

598 layer $PM_{2.5}$ was 7.5 μg m^{-3} (4.0%) when hs value was 0.35 and 6.6 μg m^{-3} (3.5%) when

599 *hs* was 0.96.

6. Conclusions

In this study, a fully coupled online WRF-Chem model with an improved integrated process rate (IPR) analysis scheme is employed to investigate the direct radiative effects (DRE) of BC vertical profiles on meteorology and $PM_{2.5}$ concentrations during two severe haze events (11-12 December 2016 and 16-19 December 2016). Sensitivity experiments are conducted to compare the DRE of BC with original and corrected vertical profiles and to quantify the role of BC vertical profiles in influencing meteorological conditions and air pollutants.

Compared to the measured vertical profiles of BC in Beijing, the default vertical profiles of BC from the WRF-Chem model can capture the decreases of BC mass concentration with altitude on December 12 and 16-19 when local emissions dominated, but cannot reproduce the observed maximum mass concentration of BC around 850-m altitude on December 11 when regional transport of pollutants dominated. Averaged over the two severe pollution events, the model overestimated BC mass concentration by 87.4% at the surface but underestimated BC by 33.1% at 1000-m altitude compared with the observations in Beijing.

We carried out simulations with both the default original BC vertical profiles and the modified vertical profiles using the observations (keep the column burden of BC from the WRF-Chem but distribute BC mass vertically according to the observed fractions of BC in individual model layers for each day). Compared with the simulation with original BC profiles, the warming by BC DRE around 300-m altitude was stronger with the modified profiles. Accordingly, the BC-induced reductions in PBLH in Beijing

averaged over the two severe haze events were 43.4 m (18.4%) and 55.4 m (23.5%), respectively, with the original and modified profiles. As a result, relative to the simulation with the original profiles, the modified profiles of BC led to larger increases in $PM_{2.5}$ concentrations by BC DRE, because VMIX and CHEM had the dominant positive contributions to the changes in surface-layer $PM_{2.5}$ due to the reductions in PBLH.

Seven sensitivity experiments were further carried out to understand the roles of BC vertical profiles. In six assumed exponential functions ($C(h)=C_0\times e^{-h/hs}$) with hs values of 0.35, 0.48, 0.53, 0.79, 0.82 and 0.96, a larger hs means less BC at the surface and more BC in the upper atmosphere. As a result, with higher hs, temperatures were less warming or even cooling occurred at the surface, leading to stronger temperature inversion as well as larger BC-induced increases in $PM_{2.5}$.

Results from our study highlight the importance of accurate representation of BC vertical profiles in models, which alter the radiation balance, BC-PBL interaction, and hence the simulated $PM_{2.5}$ concentrations. Due to the limitation of observational data, this study was focused on the DRE of BC vertical profiles on meteorology and $PM_{2.5}$ concentration in Beijing during severe haze events. However, the results from this study should be generally important for understanding severe haze for urban areas.

There are channels for further improvement in near-future research. We distribute BC mass vertically according to the observed fractions of BC in individual model layers for each day without considering the hourly variations of BC vertical profiles due to the lack of data. Such assumed distribution of BC based on observation may not be

644   consistent with the dynamical (winds, temperature, etc.) and chemical processes of the

645   atmosphere. Further efforts are needed to examine the roles of BC vertical profiles in

646   coupled chemistry-weather models.

647

648 ***Data availability.***

649 The WRF-Chem model is available at

650 https://www2.mmm.ucar.edu/wrf/users/downloads.html (last access: 7 July 2020).

651 The observations and simulation results are available upon request from the

652 corresponding author (hongliao@nuist.edu.cn).

653

654 ***Competing interests.***

655 The authors declare that they have no conflict of interest.

656

657 ***Author contributions.***

658 DC and HL designed the study and DC wrote the paper. DC performed model

659 simulations and analyzed the data. DZ and DD provided the observed data. YY and LC

660 provided technical support.

661

662 ***Acknowledgements.***

663 This work was supported by the National Key Research and Development Program of

664 China (grant no. 2019YFA0606804), the National Natural Science Foundation of China

665 (grant no. 42021004), and the Major Research Plan of the National Social Science

666 Foundation (grant no.18ZDA052).

667

668

References

Barnard, J. C., Fast, J. D., Paredesmiranda, G., Arnott, W. P., and Laskin, A.: Technical Note: Evaluation of the WRF-Chem "Aerosol Chemical to Aerosol Optical Properties" Module using data from the MILAGRO campaign, Atmos. Chem. Phys., 10, 7325-7340, https://doi.org/10.5194/acp-10-7325-2010, 2010.

Bond, T. C., Doherty, S. J., Fahey, D. W., Forster, P. M., Berntsen, T., Deangelo, B., Flanner, M. G., Ghan, S. J., Karcher, B., and Koch, D.: Bounding the role of black carbon in the climate system: A scientific assessment, J. Geophys. Res.-Atmos., 118, 5380-5552, https://doi.org/10.1002/jgrd.50171, 2013.

Cappa, C.D., Onasch, T.B., Massoli, P., Worsnop, D.R., Bates, T.S., Cross, E.S., Davidovits, P., Hakala, J., Hayden, K.L., Jobson, B.T., Kolesar, K.R., Lack, D.A., Lerner, B.M., Li, S.-M., Mellon, D., Nuaaman, I., Olfert, J.S., Petäjä, T., Quinn, P.K., Song, C., Subramanian, R., Williams, E.J., Zaveri, R.A.: Radiative absorption enhancements due to the mixing state of atmospheric black carbon, Science, 337, 1078–1081, https://doi.org/10.1126/science.1223447, 2012.

Chen, D., Liao, H., Yang, Y., Chen, L., and Wang, H.: Simulated aging processes of black carbon and its impact during a severe winter haze event in the Beijing-Tianjin-Hebei region, Sci. Total Environ., 755, p.142712, https://doi.org/10.1016/j.scitotenv.2020.142712, 2021.

Chen, L., Zhu, J., Liao, H., Gao, Y., Qiu, Y., Zhang, M., Liu, Z., Li, N., and Wang, Y.: Assessing the formation and evolution mechanisms of severe haze pollution in the Beijing–Tianjin–Hebei region using process analysis, Atmos. Chem. Phys., 19, 10845-10864, https://doi.org/10.5194/acp-19-10845-2019, 2019.

Chu, Y., Li, J., Li, C., Tan, W., Su, T., and Li, J.: Seasonal and diurnal variability of planetary boundary layer height in Beijing: Intercomparison between MPL and WRF results, Atmos. Res., 227, 1-13, https://doi.org/10.1016/j.atmosres.2019.04.017, 2019.

Dai, H., Zhu, J., Liao, H., Li, J., Liang, M., Yang, Y., and Yue, X.: Co-occurrence of ozone and PM2.5 pollution in the Yangtze River Delta over 2013–2019:

Spatiotemporal distribution and meteorological conditions, Atmos. Res., 249, 105363, https://doi.org/10.1016/j.atmosres.2020.105363, 2021.

Ding, A. J., Huang, X., Nie,W., Sun, J. N., Kerminen, V. M., Petäjä, T., Su, H., Cheng, Y. F., Yang, X. Q., Wang, M. H., Chi, X. G., Wang, J. P., Virkkula, A., Guo, W. D., Yuan, J., Wang, S. Y., Zhang, R. J., Wu, Y. F., Song, Y., Zhu, T., Zilitinkevich, S., Kulmala, M., and Fu, C. B.: Enhanced haze pollution by black carbon in megacities in China, Geophys. Res. Lett., 43, 2873–2879, https://doi.org/10.1002/2016gl067745, 2016.

Ding, Q., Sun, J., Huang, X., Ding, A., Zou, J., Yang, X., and Fu, C.: Impacts of black carbon on the formation of advection–radiation fog during a haze pollution episode in eastern China, Atmos. Chem. Phys., 19, 7759-7774, https://doi.org/10.5194/acp-19-7759-2019, 2019a.

Ding, S., Liu, D., Zhao, D., Hu, K., Tian, P., Zhou, W., Huang, M., Yang, Y., Wang, F., and Sheng, J.: Size-Related Physical Properties of Black Carbon in the Lower Atmosphere over Beijing and Europe, Environ. Sci. Technol., 53, 11112-11121, https://doi.org/10.1021/acs.est.9b03722, 2019b.

Duan, J., Huang, R.-J., Lin, C., Dai, W., Wang, M., Gu, Y., Wang, Y., Zhong, H., Zheng, Y., Ni, H., Dusek, U., Chen, Y., Li, Y., Chen, Q., Worsnop, D. R., O'Dowd, C. D., and Cao, J.: Distinctions in source regions and formation mechanisms of secondary aerosol in Beijing from summer to winter, Atmos. Chem. Phys., 19, 10319-10334, https://doi.org/10.5194/acp-19-10319-2019, 2019.

Elser, M., Huang, R.-J., Wolf, R., Slowik, J. G., Wang, Q., Canonaco, F., Li, G., Bozzetti, C., Daellenbach, K. R., Huang, Y., Zhang, R., Li, Z., Cao, J., Baltensperger, U., El-Haddad, I., and Prévôt, A. S. H.: New insights into PM2:5 chemical composition and sources in two major cities in China during extreme haze events using aerosol mass spectrometry, Atmos. Chem. Phys., 16, 3207–3225, https://doi.org/10.5194/acp-16-3207-2016, 2016.

Emmons, L. K., Walters, S., Hess, P. G., Lamarque, J., Pfister, G., Fillmore, D., Granier, C., Guenther, A., Kinnison, D. E., and Laepple, T.: Description and evaluation of the Model for Ozone and Related chemical Tracers, version 4 (MOZART-4),

728   Geosci. Model Dev., 3(1), 43-67, https://doi.org/10.5194/gmd-3-43-2010, 2010.

729 Ferrero, L., Castelli, M., Ferrini, B., Moscatelli, M., Perrone, M., Sangiorgi, G.,

730   Dangelo, L., Rovelli, G., Moroni, B., Scardazza, F.: Impact of black carbon aerosol

731   over Italian basin valleys: high-resolution measurements along vertical profiles,

732   radiative forcing and heating rate, Atmos. Chem. Phys., 14, 9641–9664,

733   https://doi.org/10.5194/acp-14-9641-2014, 2014.

734 Gao, J., Zhu, B., Xiao, H., Kang, H., Hou, X., Yin, Y., Zhang, L., and Miao, Q.: Diurnal

735   variations and source apportionment of ozone at the summit of Mount Huang, a

736   rural   site   in   Eastern   China,   Environ.   Pollut.,   222,   513–522,

737   https://doi.org/10.1016/j.envpol.2016.11.031, 2017.

738 Gao, J., Zhu, B., Xiao, H., Kang, H., Pan, C., Wang, D., and Wang, H.: Effects of black

739   carbon and boundary layer interaction on surface ozone in Nanjing, China, Atmos.

740   Chem. Phys., 18, 7081-7094, https://doi.org/10.5194/acp-18-7081-2018, 2018.

741 Gao, M., Carmichael, G. R., Wang, Y., Ji, D., Liu, Z., and Wang, Z.: Improving

742   simulations of sulfate aerosols during winter haze over Northern China: the

743   impacts of heterogeneous oxidation by NO_2, Front. Environ. Sci. Technol., 10(5),

744   1-11, https://doi.org/10.1007/s11783-016-0878-2, 2016a.

745 Gao, M., Carmichael, G. R., Wang, Y., Saide, P. E., Yu, M., Xin, J., Liu, Z., and Wang,

746   Z.: Modeling study of the 2010 regional haze event in the North China Plain,

747   Atmos. Chem. Phys., 16, 1673-1691, https://doi.org/10.5194/acp-16-1673-2016,

748   2016b.

749 Grell, G. A., Peckham, S. E., Schmitz, R., Mckeen, S. A., Frost, G. J., Skamarock, W.

750   C., and Eder, B.: Fully coupled "online" chemistry within the WRF model, Atmos.

751   Environ., 39, 6957-6975, https://doi.org/10.1016/j.atmosenv.2005.04.027, 2005.

752 Guenther, A., Karl, T., Harley, P., Wiedinmyer, C., Palmer, P. I. and Geron, C.: Estimates

753   of global terrestrial isoprene emissions using MEGAN (Model of Emissions of

754   Gases and Aerosols from Nature), Atmos. Chem. Phys., 6(11), 3181–3210,

755   https://doi.org/10.5194/acp-6-3181-2006, 2006.

756 He, J., Gong, S., Yu, Y., Yu, L., Wu, L., Mao, H., Song, C., Zhao, S., Liu, H., and Li,

757   X.: Air pollution characteristics and their relation to meteorological conditions

during 2014–2015 in major Chinese cities, Environ. Pollut., 223, 484-496, https://doi.org/ 10.1016/j.envpol.2017.01.050, 2017.

Hong, S., Noh, Y., and Dudhia, J.: A New Vertical Diffusion Package with an Explicit Treatment of Entrainment Processes, Mon. Weather Rev., 134, 2318-2341, https://doi.org/10.1175/MWR3199.1, 2006.

Hu, K., Zhao, D., Liu, D., Ding, S., Tian, P., Yu, C., Zhou, W., Huang, M., and Ding, D.: Estimating radiative impacts of black carbon associated with mixing state in the lower atmosphere over the northern North China Plain, Chemosphere, 252, https://doi.org/10.1016/j.chemosphere.2020.126455, 2020.

Huang, X., Ding, A., Gao, J., Zheng, B., Zhou, D., Qi, X., Tang, R., Wang, J., Ren, C., Nie, W., Chi, X., Xu, Z., Chen, L., Li, Y., Che, F., Pang, N., Wang, H., Tong, D., Qin, W., Cheng, W., Liu, W., Fu, Q., Liu, B., Chai, F., Davis, S. J., Zhang, Q., and He, K.: Enhanced secondary pollution offset reduction of primary emissions during COVID-19 lockdown in China, Natl. Sci. Rev., nwaa137, https://doi.org/10.31223/OSF.IO/HVUZY, 2020.

Huang, X., Song, Y., Zhao, C., Cai, X., Zhang, H., and Zhu, T.: Direct Radiative Effect by Multicomponent Aerosol over China, J. Climate, 28, 3472-3495, https://doi.org/10.1175/JCLI-D-14-00365.1, 2015.

Huang, X., Wang, Z., and Ding, A.: Impact of Aerosol-PBL Interaction on Haze Pollution: Multiyear Observational Evidences in North China, Geophys. Res. Lett., 45, 8596-8603, https://doi.org/10.1029/2018GL079239, 2018.

Ji, D., Li, L., Pang, B., Xue, P., Wang, L., Wu, Y., Zhang, H., and Wang, Y.: Characterization of black carbon in an urban-rural fringe area of Beijing, Environ. Pollut., 223, 524–534, https://doi.org/10.1016/j.envpol.2017.01.055, 2017.

Jiang, F., Zhou, P., Liu, Q., Wang, T., Zhuang, B., and Wang, X.: Modeling tropospheric ozone formation over East China in springtime, J. Atmos. Chem., 69(4), 303-319, https://doi.org/10.1007/s10874-012-9244-3, 2012.

Khor, W. Y., Hee, W. S., Tan, F., San Lim, H., Jafri, M. Z. M., and Holben, B.: Comparison of Aerosol optical depth (AOD) derived from AERONET sunphotometer and Lidar system, IOP Conf. Ser.: Earth Environ. Sci., 20,

788   https://doi.org/10.1088/1755-1315/20/1/012058, 2014.

789   Kong, S., Li, X., Li, L., Yin, Y., Chen, K., Yuan, L., Zhang, Y., Shan, Y., and Ji, Y.:

790   Variation of polycyclic aromatic hydrocarbons in atmospheric PM2.5 during

791   winter haze period around 2014 Chinese Spring Festival at Nanjing: Insights of

792   source changes, air mass direction and firework particle injection, Sci. Total

793   Environ., 520, 59–72, https://doi.org/10.1016/j.scitotenv.2015.03.001, 2015.

794   Li, J., Liao, H., Hu, J., and Li, N.: Severe particulate pollution days in China during

795   2013-2018 and the associated typical weather patterns in Beijing-Tianjin-Hebei

796   and the Yangtze River Delta regions, Environ. Pollut., 248, 74–81, https://doi.org/

797   10.1016/j.envpol.2019.01.124, 2019.

798   Li, K., Jacob, D. J., Liao, H., Zhu, J., Shah, V., Shen, L., Bates, K. H., Zhang, Q., and

799   Zhai, S.: A two-pollutant strategy for improving ozone and particulate air quality

800   in China, Nat. Geosci., 12, 906-910, https://doi.org/10.1038/s41561-019-0464-x,

801   2019.

802   Li, K., Liao, H., Zhu, J., and Moch, J. M.: Implications of RCP emissions on future

803    $PM_{2.5}$ air quality and direct radiative forcing over China, J. Geophys. Res.-Atmos.,

804   121, https://doi.org/10.1002/2016JD025623, 2016.

805   Li, M., Zhang, Q., Kurokawa, J., Woo, J., He, K. B., Lu, Z., Ohara, T., Song, Y., Streets,

806   D. G., and Carmichael, G. R.: MIX: a mosaic Asian anthropogenic emission

807   inventory for the MICS-Asia and the HTAP projects, Atmos. Chem. Phys., 15,

808   34813-34869, https://doi.org/10.5194/acpd-15-34813-2015, 2015.

809   Liu, D., Zhao, D., Xie, Z., Yu, C., Chen, Y., Tian, P., Ding, S., Hu, K., Lowe, D., Liu,

810   Q., Zhou, W., Wang, F., Sheng, J., Kong, S., Hu, D., Wang, Z., Huang, M., and

811   Ding, D.: Enhanced heating rate of black carbon above the planetary boundary

812   layer over megacities in summertime, Environ, Res, Lett., 14,

813   https://doi.org/10.1088/1748-9326/ab4872, 2019.

814   Liu, Q., Liu, D., Gao, Q., Tian, P., Wang, F., Zhao, D., Bi, K., Wu, Y., Ding, S., and Hu,

815   K.: Vertical characteristics of aerosol hygroscopicity and impacts on optical

816   properties over the North China Plain during winter, Atmos. Chem. Phys., 1-34,

817   https://doi.org/10.5194/acp-20-3931-2020, 2020.

818 Liu, T., Gong, S., He, J., Yu, M., Wang, Q., Li, H., Liu, W., Zhang, J., Li, L., Wang, X.,

819   Zhang, J., Li, L., Wang, X., Li, S., Lu, Y., Du, H., Wang, Y., Zhou, C., Liu, H., and

820   Zhao, Q.: Attributions of meteorological and emission factors to the 2015 winter

821   severe haze pollution episodes in China's Jing-Jin-Ji area, Atmos. Chem. Phys., 17,

822   2971-2980, https://doi.org/10.5194/acp-17-2971-2017, 2017.

823 Luan, T., Guo, X., Guo, L., and Zhang, T.: Quantifying the relationship between PM2.5

824   concentration, visibility and planetary boundary layer height for long-lasting haze

825   and fog–haze mixed events in Beijing, Atmos. Chem. Phys., 18, 203-225,

826   https://doi.org/10.5194/acp-18-203-2018, 2018.

827 Miao, Y., Guo, J., Liu, S., Liu, H., Li, Z., Zhang, W., and Zhai, P.: Classification of

828   summertime synoptic patterns in Beijing and their associations with boundary

829   layer structure affecting aerosol pollution, Atmos. Chem. Phys., 17, 3097-3110,

830   https://doi.org/10.5194/acp-17-3097-2017, 2017.

831 Qiu, Y., Liao, H., Zhang, R., and Hu, J.: Simulated impacts of direct radiative effects of

832   scattering and absorbing aerosols on surface layer aerosol concentrations in China

833   during a heavily polluted event in February 2014, J. Geophys. Res.-Atmos., 122,

834   5955-5975, https://doi.org/10.1002/2016JD026309, 2017.

835 Rolph, G. D.: Real-time Environmental Applications and Display System (READY),

836   NOAA Air Resources Laboratory, Silver Spring, MD, available at:

837   http://ready.arl.noaa.gov, 2013.

838 Skamarock, W. C., Klemp, J. B., Dudhia, J., Gill, D. O., Barker, D. M., Wang, W., and

839   Powers, J. G.: A description of the advanced research WRF version 2, NCAR Tech.

840   Note, NCAR/TN-468CSTR, Natl. Cent. Atmos. Res., Boulder, Colo, available at:

841   http://wrf-model.org/wrfadmin/publications.php (last access: 6 August 2020),

842   2008.

843 Stelson, A. W.: Urban aerosol refractive index prediction by partial molar refraction

844   approach, Environ. Sci. Technol., 24, 1676-1679,

845   https://doi.org/10.1021/es00081a008, 1990.

846 Sun, Y., Jiang, Q., Wang, Z., Fu, P., Li, J., Yang, T., and Yin, Y.: Investigation of the

847   sources and evolution processes of severe haze pollution in Beijing in January

2013, J. Geophys. Res.-Atmos., 119, 4380–4398, https://doi.org/10.1002/2014jd021641, 2014.

Sun, Y., Zhuang, G., Tang, A., Wang, Y., and An, Z.: Chemical Characteristics of $PM_{2.5}$ and PM_{10} in Haze−Fog Episodes in Beijing, Environ. Sci. Technol., 40, 3148-3155, https://doi.org/10.1021/es051533g, 2006.

Tian, P., Liu, D., Huang, M., Liu, Q., Zhao, D., Ran, L., Deng, Z. Z., Wu, Y., Fu, S., and Bi, K.: The evolution of an aerosol event observed from aircraft in Beijing: An insight into regional pollution transport, Atmos. Environ., 206, 11-20, https://doi.org/10.1016/j.atmosenv.2019.02.005, 2019.

Tian, P., Liu, D., Zhao, D., Yu, C., Liu, Q., Huang, M., Deng, Z., Ran, L., Wu, Y., and Ding, S.: In situ vertical characteristics of optical properties and heating rates of aerosol over Beijing, Atmos. Chem. Phys., 20(4), 2603-2622, https://doi.org/10.5194/acp-20-2603-2020, 2020.

Wang, H., Xue, M., Zhang, X., Liu, H., Zhou, C., Tan, S., Che, H., Chen, B., and Li, T.: Mesoscale modeling study of the interactions between aerosols and PBL meteorology during a haze episode in Jing–Jin–Ji (China) and its nearby surrounding region–Part 1: Aerosol distributions and meteorological features, Atmos. Chem. Phys., 15, 3257-3275, https://doi.org/10.5194/acp-15-3277-2015, 2015.

Wang, J., Zhao, B., Wang, S., Yang, F., Xing, J., Morawska, L., Ding, A., Kulmala, M., Kerminen, V., Kujansuu, J., Wang, Z., Ding, D., Zhang, X., Wang, H., Tian, M., Petäjä, T., Jiang, J., and Hao, J.: Particulate matter pollution over China and the effects of control policies, Sci. Total Environ., 584, 426-447, https://doi.org/10.1016/j.scitotenv.2017.01.027, 2017a.

Wang, Q., Sun, Y., Jiang, Q., Du, W., Sun, C., Fu, P., and Wang, Z.: Chemical composition of aerosol particles and light extinction apportionment before and during the heating season in Beijing, China, J. Geophys. Res. Atmos. 120, 12708-12722, https://doi.org/10.1002/2015JD023871, 2015.

Wang, Y., Ying, Q., Hu, J., and Zhang, H.: Spatial and temporal variations of six criteria air pollutants in 31 provincial capital cities in China during 2013-2014, Environ.

Int., 73, 413-422, https://doi.org/10.1016/j.envint.2014.08.016, 2014.

Wang, Z., Cao, X., Zhang, L., Notholt, J., Liu, R., and Zhang, B.: Lidar measurement of planetary boundary layer height and comparison with microwave profiling radiometer observation, Atmos. Meas. Tech., 5, 1965-1972, https://doi:10.5194/amt-5-1965-2012, 2012.

Wang, Z., Huang, X., and Ding, A.: Dome effect of black carbon and its key influencing factors: a one-dimensional modelling study, Atmos. Chem. Phys., 18, 2821-2834, https://doi.org/10.5194/acp-18-2821-2018, 2018.

Wang, Z., Huang, X., and Ding, A.: Optimization of vertical grid setting for air quality modelling in China considering the effect of aerosol-boundary layer interaction, Atmos. Environ., 210, 1-13, https://doi.org/10.1016/j.atmosenv.2019.04.042, 2019.

Watsonparris, D., Schutgens, N., Reddington, C. L., Pringle, K. J., Liu, D., Allan, J. D., Coe, H., Carslaw, K. S., and Stier, P.: In situ constraints on the vertical distribution of global aerosol, Atmos. Chem. Phys., 19, 11765-11790, https://doi.org/10.5194/acp-19-11765-2019, 2019.

Wiedinmyer, C., Akagi, S. K., Yokelson, R. J., Emmons, L. K., Alsaadi, J. A., Orlando, J. J., and Soja, A. J.: The Fire INventory from NCAR (FINN): a high resolution global model to estimate the emissions from open burning, Geosci. Model Dev., 4, 625-641, https://doi.org/10.5194/gmd-4-625-2011, 2011.

Wilcox, E. M., Thomas, R., Praveen, P. S., Pistone, K., Bender, F. A. M., and Ramanathan, V.: Black carbon solar absorption suppresses turbulence in the atmospheric boundary layer, Proc. Natl. Acad. Sci. USA, 113, 11794-11799, https://doi.org/10.1073/pnas.1525746113, 2016.

Wild, O., Zhu, X., and Prather, M. J.: Fast-J: Accurate Simulation of In- and Below-Cloud Photolysis in Tropospheric Chemical Models, J. Atmos. Chem., 37, 245-282, https://doi.org/10.1023/A:1006415919030, 2000.

Yang, Y., Smith, S., Wang, H., Lou, S., and Rasch, P.: Impact of Anthropogenic Emission Injection Height Uncertainty on Global Sulfur Dioxide and Aerosol Distribution, J. Geophys. Res.-Atmos., 124, 4812-4826,

908   https://doi.org/10.1029/2018JD030001, 2019.

909 Zaveri, R. A., and Peters, L. K.: A new lumped structure photochemical mechanism for

910   large-scale applications, J. Geophys. Res.-Atmos., 104, 30387-30415,

911   https://doi.org/10.1029/1999JD900876, 1999.

912 Zaveri, R. A., Easter, R. C., Fast, J. D., and Peters, L. K.: Model for Simulating Aerosol

913   Interactions and Chemistry (MOSAIC), J. Geophys. Res., 113, -,

914   https://doi.org/10.1029/2007JD008782, 2008.

915 Zhang, H., Wang, S., Hao, J., Wang, X., Wang, S., Chai, F., and Li, M.: Air pollution

916   and control action in Beijing, J. Clean. Prod., 112, 1519-1527,

917   https://doi.org/10.1016/j.jclepro.2015.04.092, 2016.

918 Zhang, J., and Rao, S. T.: The Role of Vertical Mixing in the Temporal Evolution of

919   Ground-Level Ozone Concentrations, J. Appl. Meteorol., 38, 1674-1691,

920   https://doi.org/10.1175/1520-0450(1999)038<1674:TROVMI>2.0.CO;2, 1999.

921 Zhang, J., Sun, Y., Liu, Z., Ji, D., Hu, B., Liu, Q., and Wang, Y.: Characterization of

922   submicron aerosols during a month of serious pollution in Beijing, Atmos. Chem.

923   Phys., 14, 2887–2903, https://doi.org/10.5194/acp-14-2887-2014, 2014.

924 Zhang, Q., Zheng, Y., Tong, D., Shao, M., Wang, S., Zhang, Y., Xu, X., Wang, J., He,

925   H., Liu, W., Ding, Y., Lei, Y., Li, J., Wang, Z., Zhang, X., Wang, Y., Cheng, J., Liu,

926   Y., Shi, Q., Yan, L., Geng, G., Hong, C., Li, M., Liu, F., Zheng, B., Cao, J., Fu, Q.,

927   Huo, J., Liu, B., Liu, Z., Yang, F., He, K., and Hao, J.: Drivers of improved $PM_{2.5}$

928   air quality in China from 2013 to 2017, Proc. Natl. Acad. Sci. USA, 116, 24463-

929   24469, https://doi.org/10.1073/pnas.1907956116, 2019.

930 Zhang, Y., Chen, Y., Sarwar, G., and Schere, K.: Impact of gas-phase mechanisms on

931   Weather Research Forecasting Model with Chemistry (WRF/Chem) predictions:

932   Mechanism implementation and comparative evaluation, J. Geophys. Res.-Atmos.,

933   117, https://doi.org/10.1029/2011JD015775, 2012.

934 Zhao, C., Liu, X., Ruby Leung, L., and Hagos, S.: Radiative impact of mineral dust on

935   monsoon precipitation variability over West Africa, Atmos. Chem. Phys., 11,

936   1879–1893, https://doi.org/10.5194/acp-11-1879-2011, 2011.

937 Zhao, D., Huang, M., Liu, D., Ding, D., Tian, P., Liu, Q., Zhou, W., Sheng, J., Wang,

F., Bi, K., Yang, Y., Li, X., Hu, Y., Guo, X., Gao, Y., He, H., Chen, Y., Kong, S., and Huang, J.: Aircraft measurements of black carbon in the boundary layer over the North China Plain, Atmos. Chem. Phys., 1-25, https://doi.org/10.5194/acp-2017-1118, 2018.

Zhao, D., Huang, M., Tian, P., He, H., Lowe, D., Zhou, W., Sheng, J., Wang, F., Bi, K., Kong, S., Yang, Y., Liu, Q., Liu, D., and Ding, D.: Vertical characteristics of black carbon physical properties over Beijing region in warm and cold seasons, Atmos. Environ., 213, 296-310, https://doi.org/10.1016/j.atmosenv.2019.06.007, 2019.

Zheng, B., Tong, D., Li, M., Liu, F., Hong, C., Geng, G., Li, H., Li, X., Peng, L., Qi, J., Yan, L., Zhang, Y., Zhao, H., Zheng, Y., He, K., and Zhang, Q.: Trends in China's anthropogenic emissions since 2010 as the consequence of clean air actions, Atmos. Chem. Phys., 18, 14095-14111, https://doi.org/10.5194/acp-18-14095-2018, 2018.

Zhu, J., Chen, L., Liao, H., Yang, H., Yang, Y., and Yue, X.: Enhanced $PM_{2.5}$ Decreases and O_3 Increases in China during COVID-19 Lockdown by Aerosol-Radiation Feedback, Geophys. Res. Lett., 48(2), https://doi.org/10.1029/2020GL090260, 2020.

957 **Table1.** Physical and chemical options for WRF/Chem.

WRF/Chem Model Configuration	Description
Microphysics scheme	Lin microphysics scheme (Wiedinmyer et al., 2011)
Longwave radiation scheme	RRTMG scheme (Zhao et al., 2011)
Shortwave radiation scheme	RRTMG scheme (Zhao et al., 2011)
Gas phase chemistry scheme	CBMZ (Zaveri and Peters, 1999)
Aerosol module	MOSAIC (Zaveri et al., 2008)
Photolysis scheme	Fast-J (Wild et al., 2000)
Boundary layer scheme	Yonsei University Scheme(YSU) (Hong et al., 2006)
Pavement parameterization scheme	Noah Land Surface Model scheme
Cumulus option	Grell 3-D ensemble scheme

958

959

960 **Table 2.** Numerical experiments. Y indicates "on", and N indicates "off".

Simulations	BC direct radiative effect (DRE)		
	DRE	BC vertical profiles for calculation of DRE	
	Turn on/off	Types description	Modified dates
CTRL	Y	Simulated by model	No modification
NoBCrad	N	Simulated by model	No modification
VerBC_obs	Y	Modified according to intraday observations	11-12 and 16-19 December
VerBC_hs1-6	Y	Modified according to $C(h)=C_0\times e^{-h/hs}$ function[a]	12 and 16-19 December
VerBC_RT	Y	Modified according to observations on 11 December 2016	12 and 16-19 December

961 [a] The values of *hs* in VerBC_hs1, VerBC_hs2, VerBC_hs3, VerBC_hs4, VerBC_hs5 and

962 VerBC_hs6 are 0.35, 0.48, 0.53, 0.79, 0.82 and 0.96, respectively.

963

964 **Table 3.** Statistical metrics for temperature at 2 m (T2; ℃), relative humidity at 2 m

965 (RH2; %), wind speed at 10 m (WS10; m s^{-1}), wind direction at 10 m (WD10, °), PBLH

966 (m), SWDOWN (W m^{-2}), PM$_{2.5}$ (μg m^{-3}), SO$_2$ (ppbv), NO$_2$ (ppbv), CO (ppmv) and O$_3$

967 (ppbv).

Variables	SIM[a]	OBS[b]	R[c]	MB[d]	NMB[e]	MFB[f]
T2 (℃)	-0.5	-0.6	0.77	0.1	-17.8%	-13.1%
RH2 (%)	52.5	55.8	0.75	-3.4	-6.0%	-0.3%
WS10 (m s^{-1})	1.8	2.3	0.52	-0.5	-20.6%	-11.5%
WD10 (°)	165.6	182.0	0.45	-16.4	-9.0%	0.7%
PBLH (m)	205.8	174.9	0.72	30.9	17.7%	72.9%
SWDOWN (W m^{-2})	86.0	100.8	0.76	-14.9	-14.8%	-17.4%
PM$_{2.5}$ (μg m^{-3})	145.6	132.3	0.77	13.2	10.0%	15.7%
SO$_2$ (ppbv)	7.9	7.8	0.38	0.1	1.4%	-2.9%
NO$_2$ (ppbv)	47.7	39.2	0.78	8.5	21.6%	20.2%
CO (ppmv)	1.8	1.9	0.73	-0.1	-4.9%	6.4%
O$_3$ (ppbv)	6.7	6.8	0.66	-0.1	-1.2%	-36.0%

968 [a,b] SIM and OBS represent the averaged model results and observations in Beijing from 11 to 19

969 December 2016.

970 [c] R is the correlation coefficient which is calculated between hourly observations and simulations

971 in Beijing from 11 to 19 December 2016, $R = \dfrac{\sum_{i=1}^{n}|(OBS_i-\overline{OBS})*(SIM_i-\overline{SIM})|}{\sqrt{\sum_{i=1}^{n}(OBS_i-\overline{OBS})^2+\sum_{i=1}^{n}(SIM_i-\overline{SIM})^2}}$, where OBS_i and

972 SIM_i are the hourly observed and simulated data in Beijing and n is the total number of hours.

973 [d] MB is the mean bias, $MB = \frac{1}{n}*\sum_{i=1}^{n}SIM_i - OBS_i$.

974 [e] NMB is the normalized mean bias, $NMB = \frac{1}{n}*\sum_{i=1}^{n}\frac{SIM_i-OBS_i}{OBS_i}*100\%$.

975 [f] MFB is the mean fraction bias, $MFB = \frac{2}{n}*\sum_{i=1}^{n}\frac{SIM_i-OBS_i}{SIM_i+OBS_i}*100\%$.

976

977
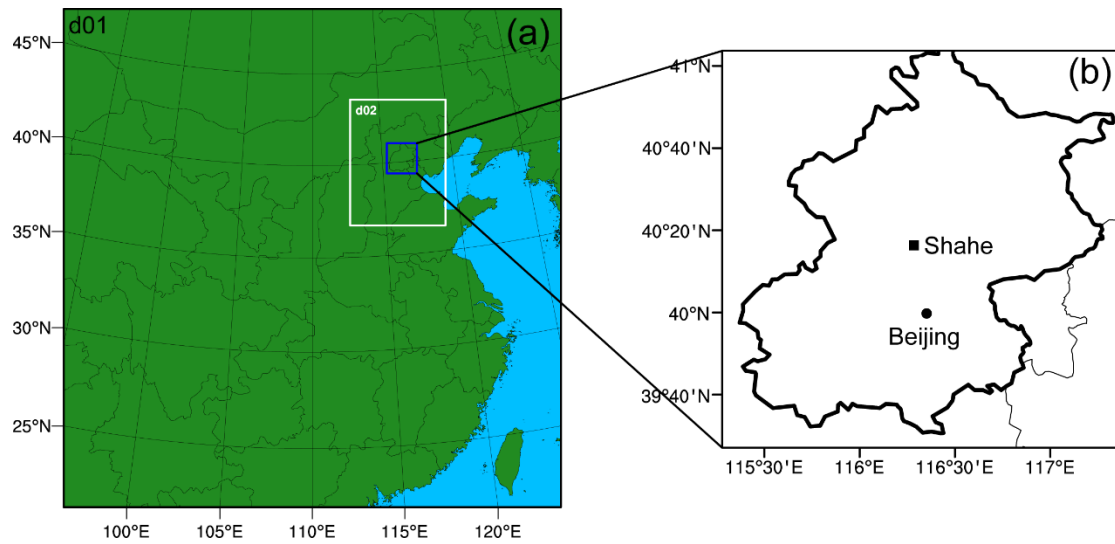
978 **Figure 1.** (a) Two nested domains with grid resolutions of 30 km (d01) and 10 km (d02).

979 (b) The BC vertical profiles were modified for the blue box which covers the whole of

980 Beijing.

981
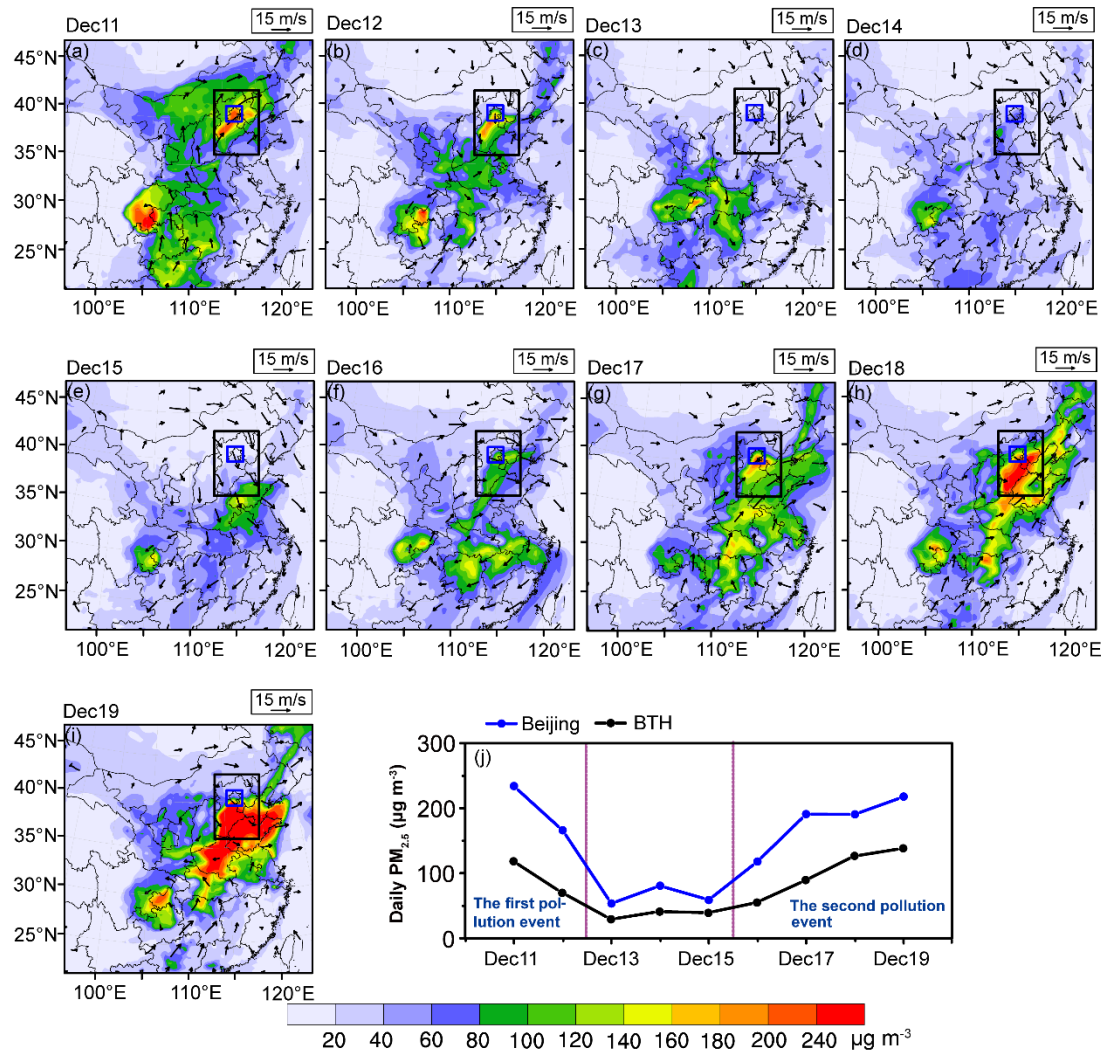
Figure 2. (a-i) Simulated spatial distributions of surface-layer PM$_{2.5}$ concentrations (μg m^{-3}) and winds (m s^{-1}) at 850 hPa at 2 pm local time from 11 to 19 December 2016. Black and blue squares in each panel denote the regions of Beijing-Tianjin-Hebei and Beijing, respectively. (j) Time series of simulated mean daily PM$_{2.5}$ concentration from 11 to 19 December 2016 averaged over the Beijing (blue square) and BTH (black square).
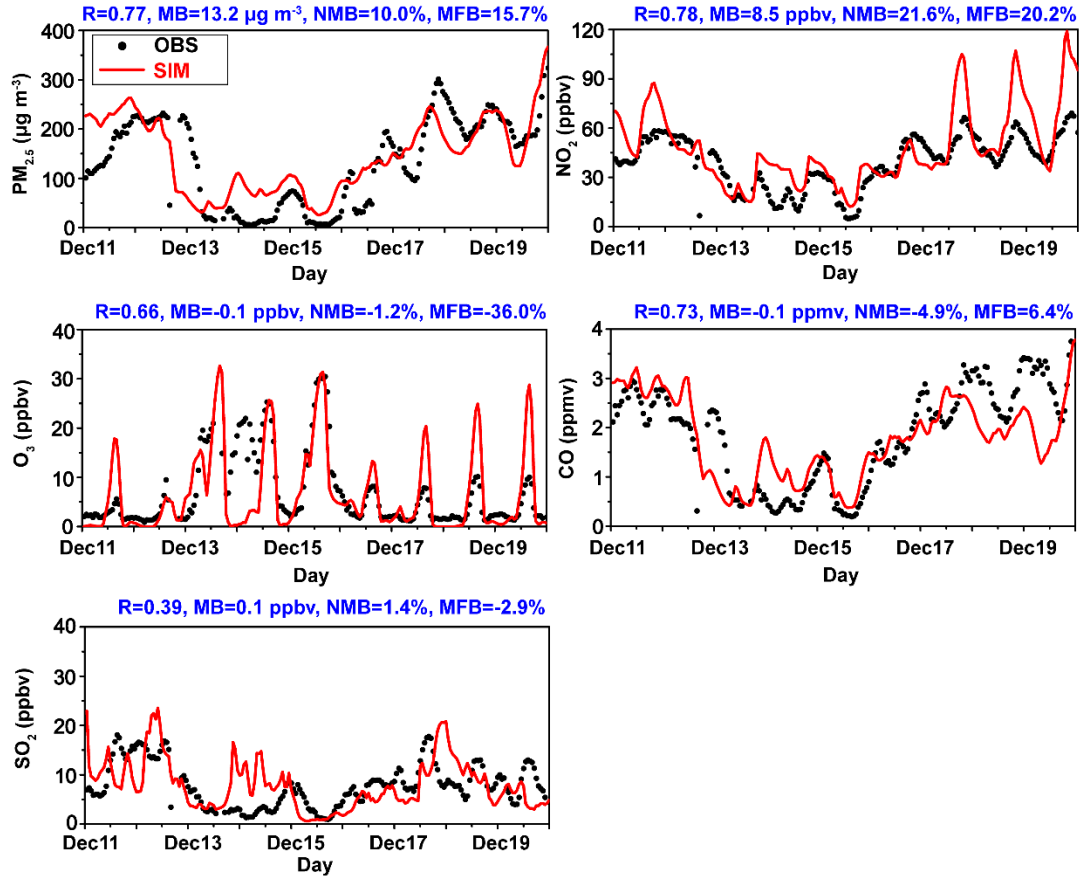
Figure 3. Time series of the observed (black dots) and simulated (red lines) hourly concentrations of $PM_{2.5}$ ($\mu g\ m^{-3}$), NO_2 (ppbv), O_3 (ppbv), CO (ppmv) and SO_2 (ppbv) in Beijing from 11 to 19 December 2016. The observations and simulations in Beijing were averaged over 12 observational sites and corresponding grid points, respectively.
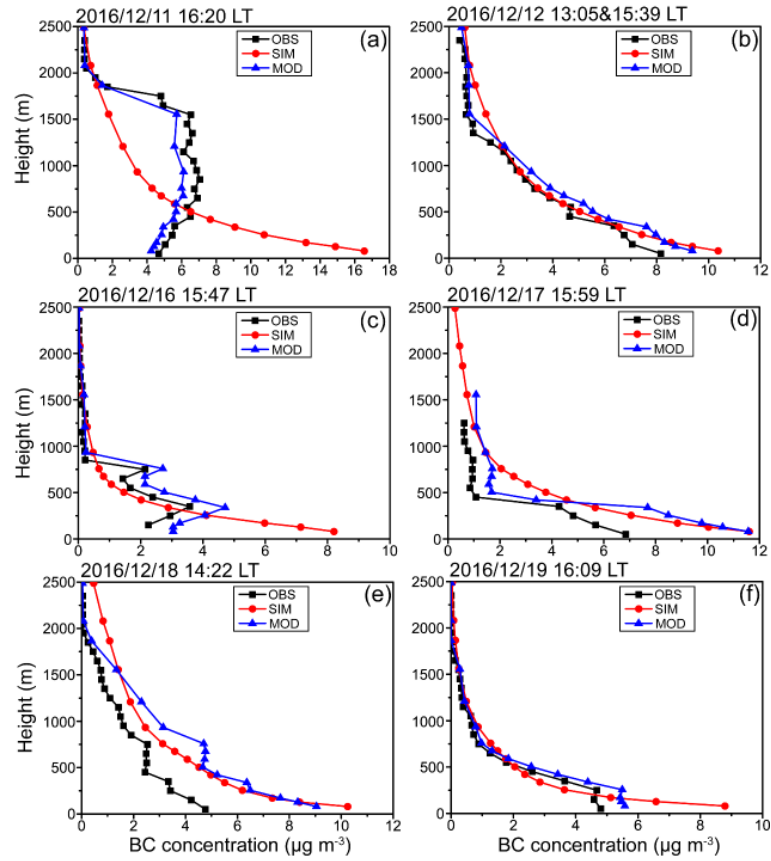
997
998 **Figure 4.** Observed (black line), simulated (red line) and modified (blue line) BC
999 vertical profiles in Beijing on 11-12 and 16-19 December 2016. The time of observation
1000 is indicated on top of each panel. The model results are two-hour averages around the
1001 observation time.
1002
1003
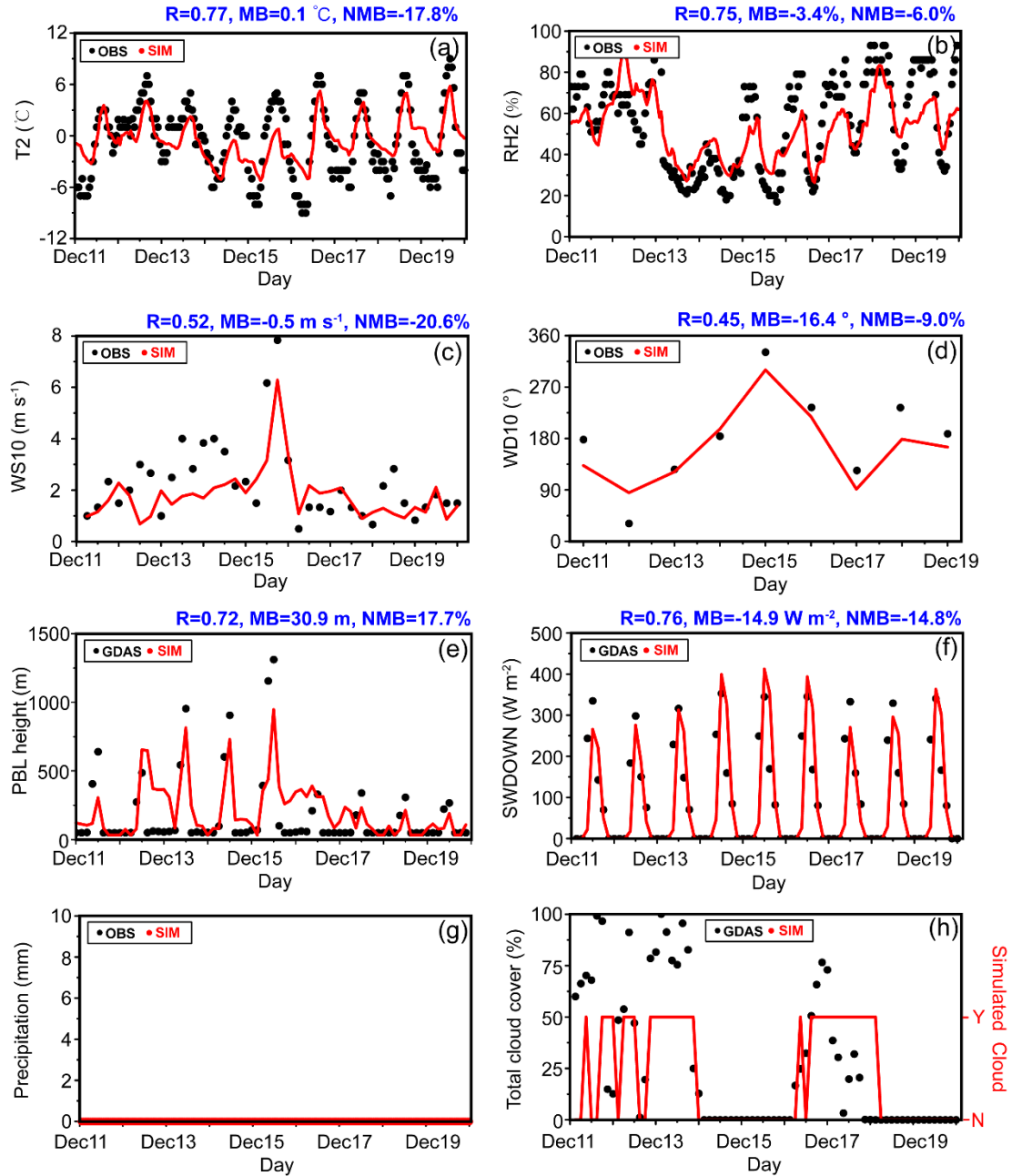
Figure 5. Comparisons of simulated meteorological parameters from CTRL simulation with measurements. The black dots and red lines are the observed (reanalysis) and simulated hourly data of T2 (℃), RH2 (%), precipitation (mm), and 3-hourly data of PBL height (m), SWDOWN (W m^{-2}), total cloud cover (%), 6-hourly data of WS10 (m s^{-1}), and daily data of WD10 (°) in Beijing from 11 December 2016 to 19 December 2016. PBLH, SWDOWN, and total cloud cover are taken from GDAS. The WRF-Chem model output shows only a grid has cloud (Y) or no cloud (N).

1014
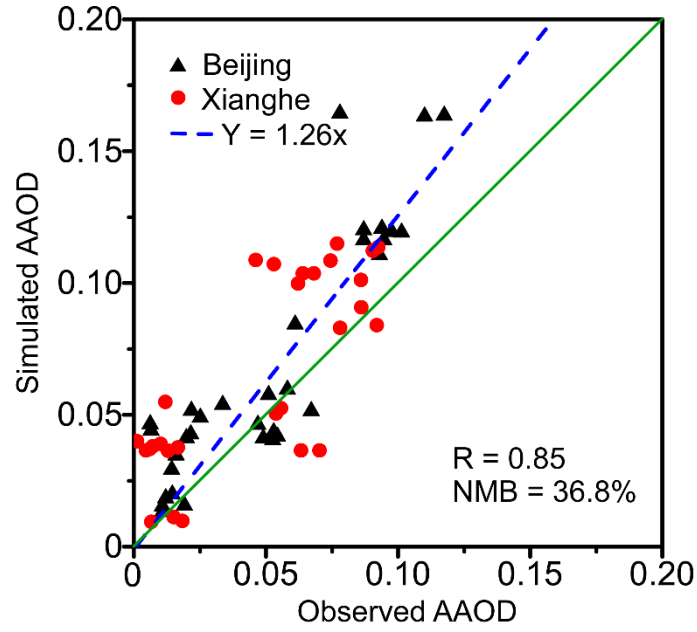
Figure 6. Comparison of simulated absorption aerosol optical depth (AAOD) at 550

nm with observations in Beijing (116.38°E, 39.98°N) and Xianghe (116.96°E, 39.75°N)

station from 11 to 19 December 2016.

1015
1016
1017
1018
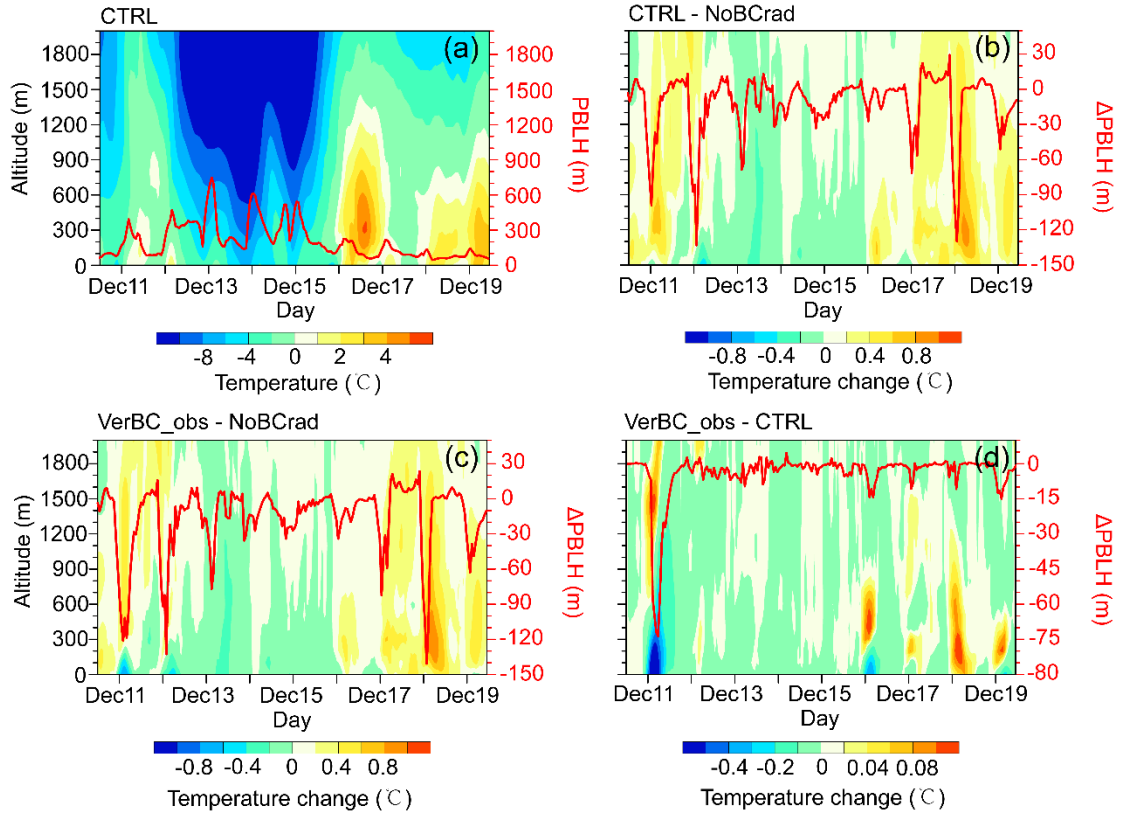
Figure 7. (a) Simulated hourly vertical profiles of temperature (contour) and PBLH (red solid line) over Beijing at local time (LT) from 11 December 2016 to 19 December 2016. (b-d) Time series of changes in vertical temperature (contour) and PBLH (ΔPBLH; red solid line) induced by BC DRE with original (b; CTRL minus NoBCrad) and modified vertical profiles (c; VerBC_obs minus NoBCrad), and the difference between the effects of modified and original BC profiles (d; VerBC_obs minus CTRL) over Beijing region from 11 December 2016 to 19 December 2016.

1028
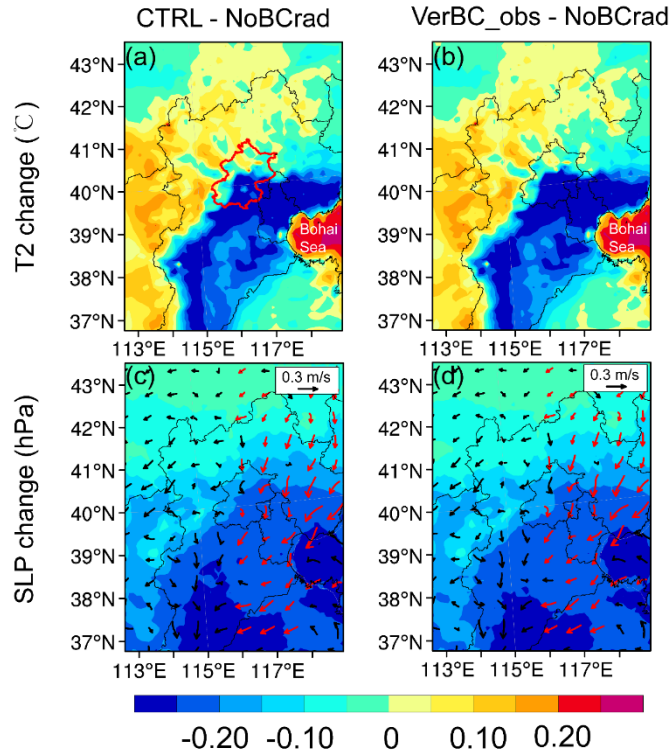
Figure 8. The changes in T2, SLP and wind at 10 m induced by BC DRE with original

(a and c; CTRL minus NoBCrad) and modified vertical profiles (b and d; VerBC_obs

minus NoBCrad) averaged over the period of 12:00 – 18:00 LT of the two haze events,

respectively. (c-d) The northeasterlies in the east of BTH are denoted in red.

1033

1034
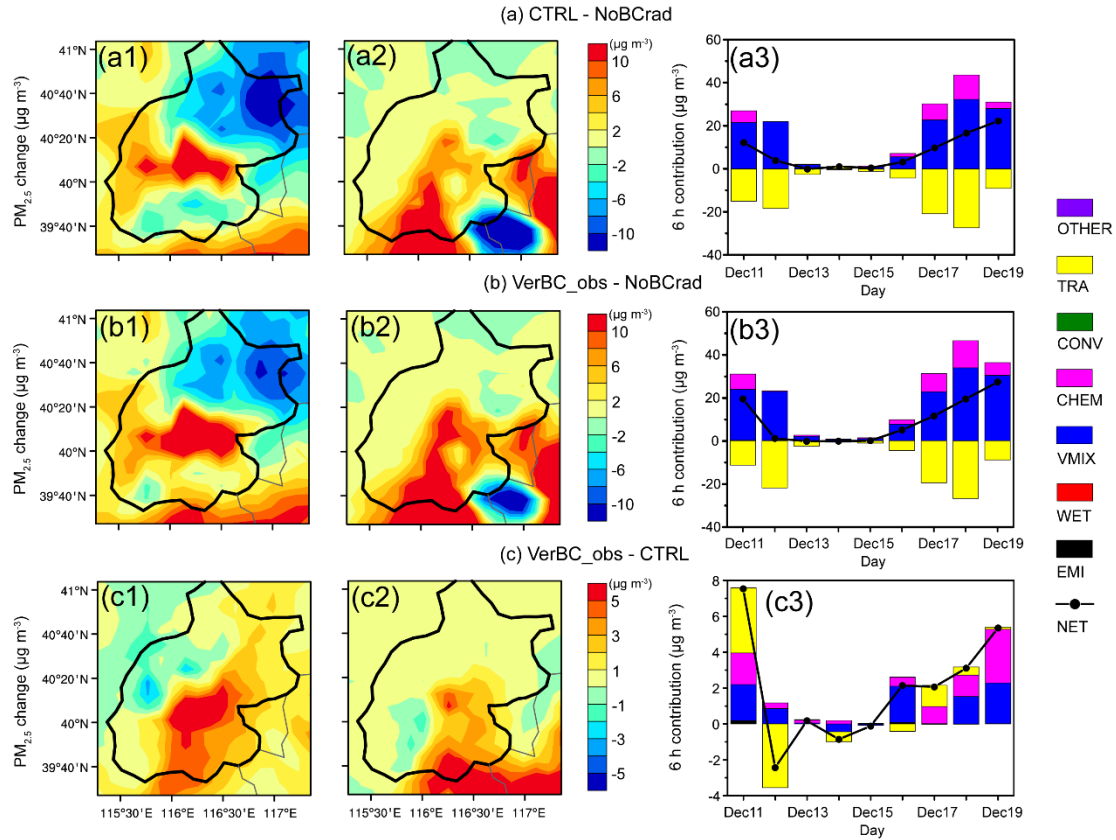
Figure 9. The spatial distribution of changes in near-surface PM$_{2.5}$ concentrations induced by BC DRE with original (CTRL minus NoBCrad; a1 and a2) and modified vertical profiles (VerBC_obs minus NoBCrad; b1 and b2), and the difference between VerBC_obs and CTRL (VerBC_obs minus CTRL; c1 and c2) over Beijing averaged over the period of 12:00 – 18:00 LT of the two haze events. a1-c1 represent the first pollution event of 11-12 December 2016 and a2-c2 represent the second pollution event of 16-19 December 2016. (a3-c3) The daily 6-h contributions of each physical/chemical process (colored bars, each of which is calculated as the concentration at 18:00 minus that at 12:00) to the change in PM$_{2.5}$ in Beijing from 11 December 2016 to 19 December 2016. The black dotted line represents the 6-h net contribution to PM$_{2.5}$ change by summing over all processes.

1046
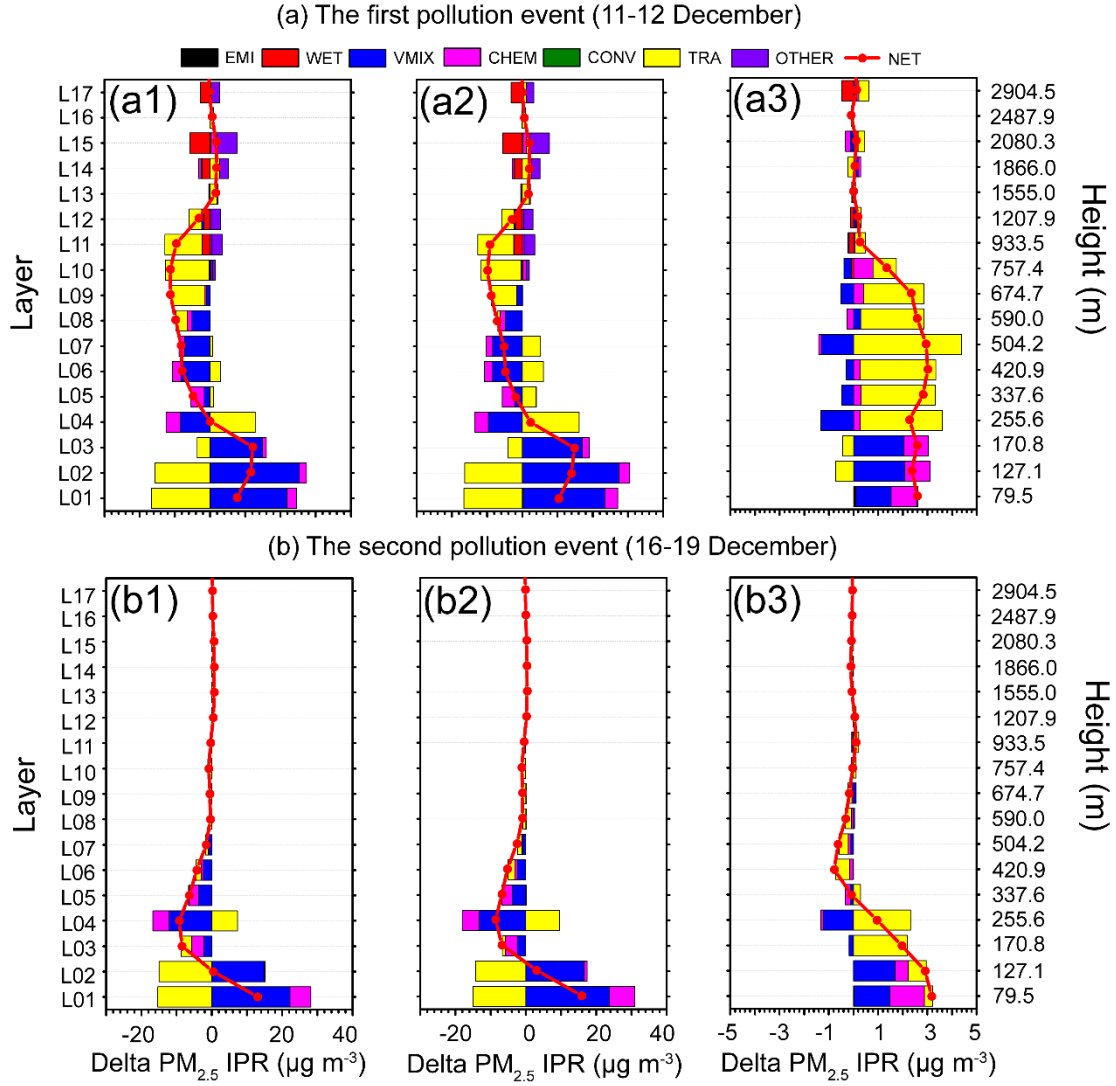
Figure 10. Vertical profiles of the 6-h contributions of physical/chemical processes (colored bars; each is calculated as the concentration at 18:00 LT minus that at 12:00 LT) to the changes in $PM_{2.5}$ induced by BC DRE with original (CTRL minus NoBCrad; a1 and b1) and modified vertical profiles (VerBC_obs minus NoBCrad; a2 and b2), and the difference between original and modified BC profiles (VerBC_obs minus CTRL; a3 and b3) over Beijing. The red dotted lines represent the 6-h net contributions to $PM_{2.5}$ changes by summing over all processes.

1056
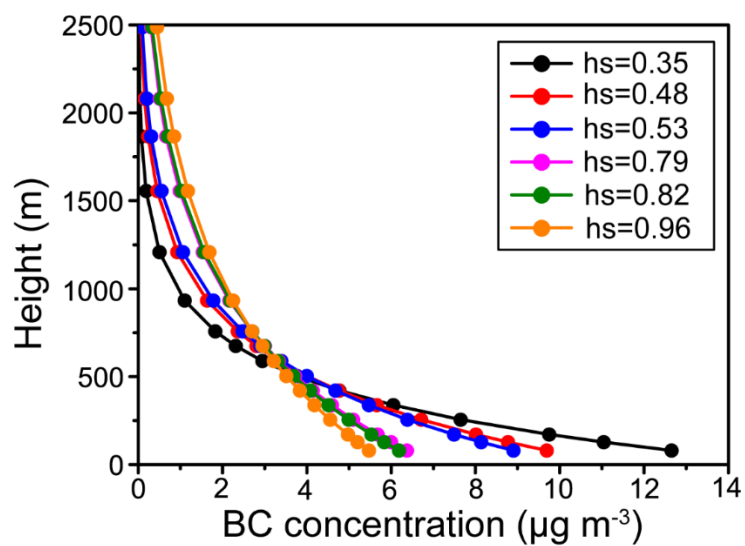
1057 **Figure 11.** Vertical profiles of BC concentrations parameterized as six exponential

1058 functions for 12 and 16-19 December 2016.

1059

1060
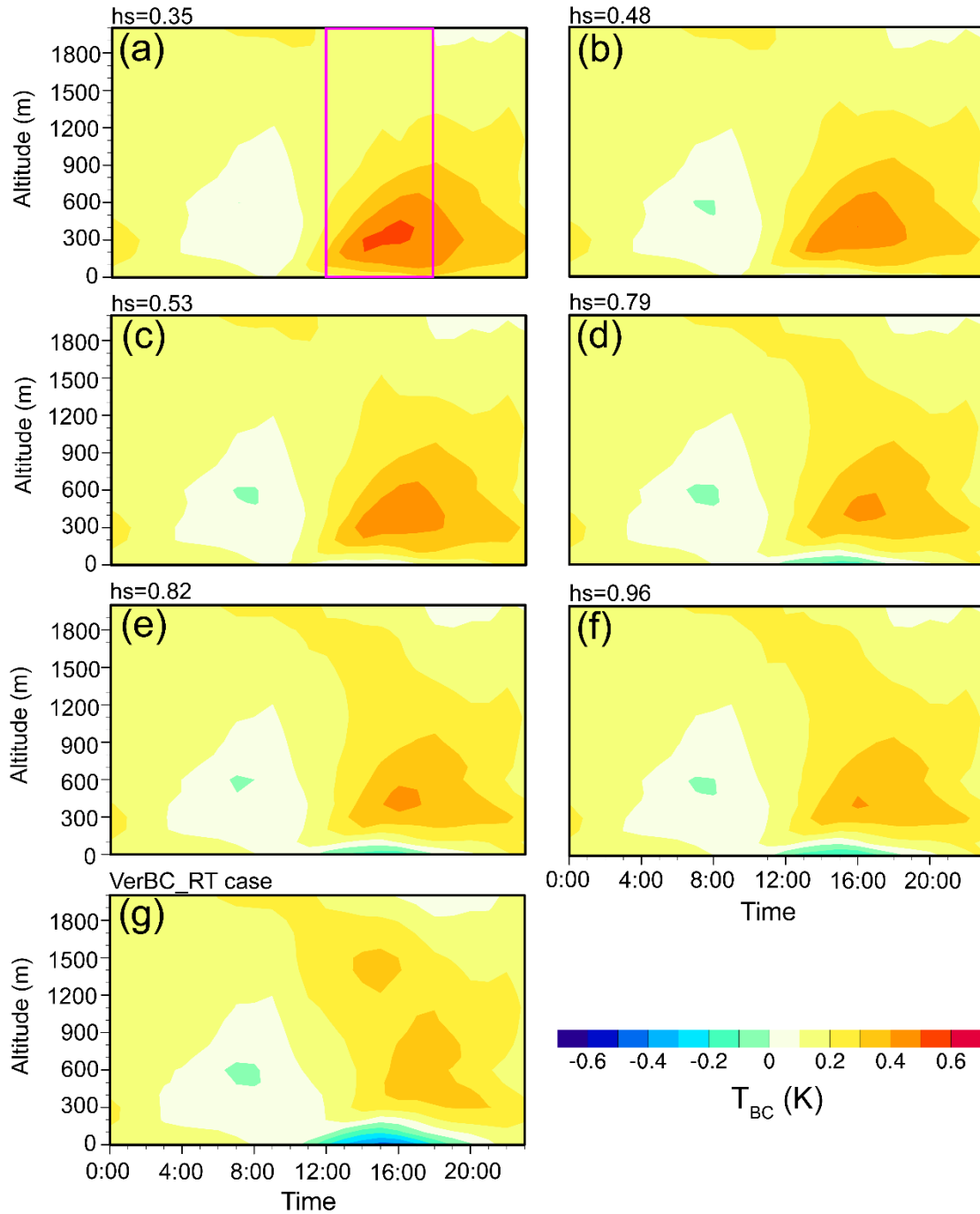
Figure 12. Time series of changes in vertical temperature induced by BC DRE with six exponential functions (VerBC_hs1-6 minus NoBCrad) and one transport-dominated vertical profile (VerBC_RT minus NoBCrad) averaged over 12 and 16-19 December 2016.

1067
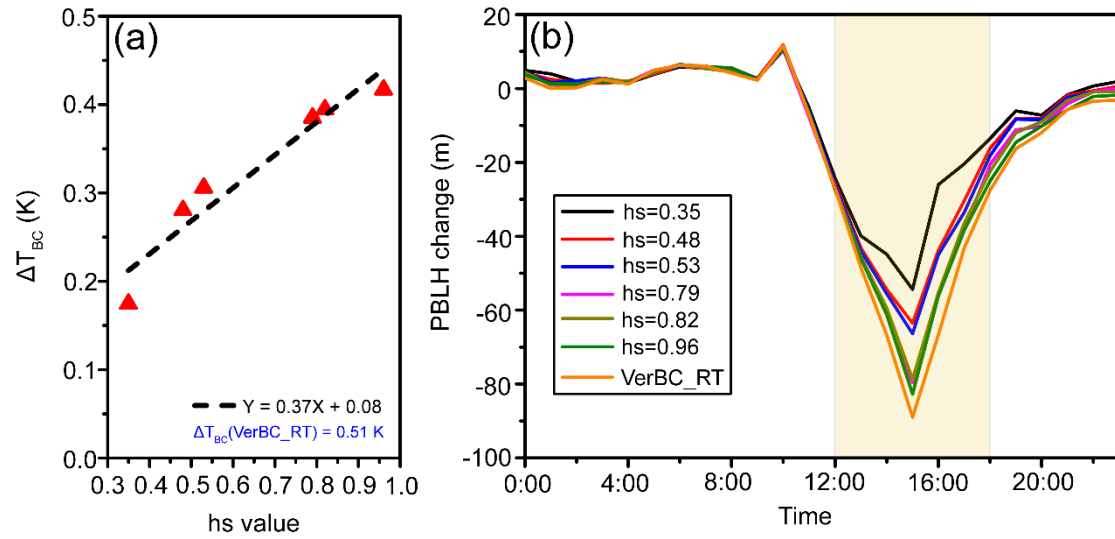
1068 **Figure 13.** (a) Variation of ΔT_{BC} caused by BC DRE with increasing *hs* values averaged

1069 12 and 16-19 December. The black dash line is the linear fit. (b) Time series of changes

1070 in PBLH in Beijing caused by different BC vertical profiles averaged 12 and 16-19

1071 December 2016.

1072

Figure 14. (a) Time series of the changes in surface-layer PM$_{2.5}$ in Beijing caused by BC with six exponential functions (VerBC_hs1-6 minus NoBCrad) and one observed transport-dominated vertical profile (VerBC_RT minus NoBCrad) averaged 12 and 16-19 December 2016. (b-d) The hourly contributions of each physical/chemical process to PM$_{2.5}$ changes caused by BC DRE with two exponential functions (*hs*=0.35 and 0.96) and one transport-dominated vertical profile.